TECHNISCHE UNIVERSITÄT MÜNCHEN

Pankreas-Forschungslabor/Chirurgische Klinik und Poliklinik

Klinikum rechts der Isar

Dominant oncogenic signal-mediated nutritional dependency affects malignant behaviours of pancreatic cancer

Ziying Jian

Vollständiger Abdruck der von der Fakultät für Medizin der Technischen Universität München zur Erlangung des akademischen Grades eines Doktors der Medizin genehmigten Dissertation.

Vorsitzender: Prof. Dr. E. J. Rummeny

Prüfer der Dissertation:

1. Prof. Dr. J. H. Kleeff (schriftliche Beurteilung)

   apl. Prof. Dr. H. Algül (mündliche Prüfung)

2. Prof. Dr. B. Holzmann

Die Dissertation wurde am 11.10.2016 bei der Technischen Universität München eingereicht und durch die Fakultät für Medizin angenommen.

Contents

ABSTRACT

Pancreatic ductal adenocarcinoma (PDAC) cells are often exposed to harsh microenvironment with particularly nutrient-limited conditions. So far, it remains unclear whether the dominant oncogenic signal is associated with the development of this nutrient-limited microenvironment.

Thus, we used two types of previously characterized murine PDAC cells (Mek/Erk- vs. PI3K/Akt-dependent) to investigate the potential link between the dominant oncogenic signal and the formation of the nutrient-limited microenvironment. Here, we observed that Mek/Erk-dependent PDAC cells require exquisitely glucose for cell expansion while the proliferation of PI3K/Akt-dependent cells depend on glutamine, showing that major energy source is indeed determined by the dominant oncogenic signal. Furthermore, nutritionally stressful condition select cancer cells with locally aggressive and angiogenic phenotype, which are paradoxically deficient in remote colonization. This loss of capacity in remote colonization is associated with an altered expression in the extracellular matrix (ECM) proteins.

Taken together, our data demonstrate a potential link between dominant oncogenic pathways, nutritional reliance and phenotypic changes of PDAC which needs to be further explored.

1. INTRODUCTION

Pancreatic cancer, one of the most devastating solid tumours, is the fourth leading cause of death among current cancer types [1]. Due to the aggressive features, over 95% of patients are already in advanced stages upon initial diagnosis, rendering the five-year survival rate lower than 5% [2]. The major pathological type of pancreatic cancer is pancreatic ductal adenocarcinoma (PDAC), which is assumed to originate from pancreas exocrine part [3]. PDAC is a highly aggressive tumour entity with rapid expansion, dense stroma, poor vascularisation and early metastasis. Recent data suggest that the malignant phenotype of PDAC is probably related to oncogene addiction and aberrant metabolic adaption [4].

1.1 Genetic mutation and gene addiction in PDAC

1.1.1 V-Ki-ras2 Kirsten rat sarcoma viral oncogene homologue (KRAS) and prominent downstream pathways

Recently, a number of oncogenic events have been demonstrated to be relevant in pancreatic carcinogenesis. Historically, it has been shown that activation of the oncogenic KRAS gene and inactivation of tumour-suppressor genes (such as p16/CDKN2A, TP53, SMAD4, ashMLH1 and MSH2) are important for PDAC initiation and development, among which the oncogenic KRAS mutation is considered to be the most pivotal event [5, 6]. In normal tissue, KRAS remains in an inactivated form by binding to guanosine diphosphate (GDP). Upon activation by upstream signals, KRAS switches from an inactivated GDP-bounding state to an activated guanosine triphosphate (GTP)-binding state. Afterwards, GTPase-activating proteins turn active KRAS

back to an inactive state. The "oncogenic" KRAS mutation often refers to a single amino acid exchange from glycine to arginine at codon 12, which leads to a persistent activation state of the KRAS, and eventually affecting the downstream pathways [7]. Recently, oncogenic KRAS gene is demonstrated as a very early genetic event during the development of PDAC. By using a number of mouse models, it has been demonstrated that the oncogenic KRAS mutation plays vital roles in the development of precancerous PanINs (Pancreatic intraepithelial neoplasms) lesions [8]. Apart from tumour initiation, the oncogenic KRAS mutations are also crucial for the tumour progression and maintenance [9].

It is well-known that oncogenic KRAS signals have a plethora of downstream pathways, two of them are proven to be highly relevant in pancreatic carcinogenesis. Here, accumulated evidence confirms that extracellular signal-regulated kinases (ERKs) cascade pathway plays a vital role in pancreatic carcinogenesis and development.

MAPK (mitogen-activated protein kinases) cascades are highly conserved pathways, which can be activated by oncogene mutation, growth factors and stresses. As a main downstream component of MAPK pathway, ERK1/2 is particularly important in regulating cell proliferation, cell cycle progression, cell survival, apoptosis, senescence, epithelial-mesenchymal transition (EMT), angiogenesis, cell invasion and metastasis; thus, ERK1/2 is validated as a gene with "oncogene function" [10, 11]. Due to the essential biological outcome, the KRAS/ERK pathway has become the focus of research in the last decades.

Apart from KRAS/ERK pathway, another important downstream pathway of oncogenic KRAS is the phosphatidylinositol-4,5-bisphosphate 3-kinase (PI3K)/protein kinase B (PI3K/AKT) pathway. The whole genome sequencing studies have shown that 10% of patients harbour aberrant alternation along the PI3K/AKT pathway [12]. When PI3K is activated, it phosphorylates phosphatidylinositides (PIP3), which further phosphorylates and activates AKT. As a key antagonist of PI3K/AKT pathway, phosphatase and tensin homologue (PTEN) dephosphorylates PIP3 to phosphatidylinositol biphosphate (PIP2) and impairs AKT ability. High levels of AKT phosphorylation are observed in PDAC patients, and it is associated with poor prognosis [13].

1.1.2 mTOR is a common downstream target of MEK/ERK and PI3K/AKT

Tumour cells are flexible in phenotypic adaptation, and they rapidly respond to nutritional alterations within the environment. The mechanistic target of rapamycin (mTOR), an environmental sensor protein, plays a critical role in translating local clues into cellular responses to maintain homoeostasis and appropriate metabolism [14]. The mTOR kinase comprises two distinct multi-proteins: mTOR complex1 (mTORC1) and mTOR complex 2 (mTORC2). In both cellular function and downstream substrates, mTORC1 and mTORC2 operate differently. Notably, mTORC1 signalling stimulates major macromolecules' biosynthesis, promotes ATP production, reduces nicotinamide adenine dinucleotide phosphate ($NADP^+$) generation, and controls intracellular anabolism and catabolism levels [15]. Unlike mTORC1, the function and regulation of mTORC2 are barely understood. Currently, it is

concluded to be related to cell turgor, membrane tension and cellular metabo-metabolism [16].

Tuberous sclerosis complex (TSC) is a negative regulator of mTOR signalling; moreover, there is a functional link between AKT with mTOR and ERK with mTOR. Activation of KRAS/ERK and PI3K/AKT can deactivate TSC operations simultaneously, impair mTOR inhibition, and promote its activation [17]. Both KRAS/ERK and PI3K/AKT pathways are crucial in regulating cell proliferation, chemo-sensitivity, motility, and metabolism [18, 19]

1.1.3   Oncogene addiction and dominant cancer signal

Despite other numerous genetic aberrations, cancer cells tend to develop a remarkable dependency on a particular oncogenic pathway for proliferation and progression [20]. This phenomenon argues for the cancerous phenotype and unique cell characteristics when responding to hostile environmental alteration. In previous decades, a growing number of studies suggest that the dominant oncogenic pathways mediated by specific gene mutations and epigenetic aberrations contribute to oncogenic addiction, which provides a rational reasoning for overcoming oncogenic addiction by targeting the dominant activated oncogenic pathway [21].

1.2 Metabolic environment in PDAC

A tumour's microenvironment is composed of endothelial cells, immune cells, neural cells, fibroblasts and many other macromolecules, such as signalling molecules, extracellular matrix (ECM) [22]. Apart from cells and macromolecules, metabolites are also crucial for regulating both tumour cell behaviour and its interaction with other environmental elements. The nutritive

material provides tumour cells with energy and molecular substrates for the thesis of large molecules which are necessary for cell proliferation and metastasis. In line, growing evidence indicates that environmental metabolic interventions may facilitate tumour progression [23]. Meanwhile, the fluctuation of nutrients select adapted clones to survive and to expand, which, in return, empowers these adapted clones with anti-apoptotic or chemoresistance [24].

The deregulating cellular energetics has been recently defined as the novel hallmark of cancer [25]. Due to the abundance of dense stromal reactions and meagre vascularisation, PDAC is characterised as heterogeneous and nutrient poor. The nutrient deprivation (such as glucose and glutamine) status makes survival conditions extremely harsh for pancreatic cancer cells. It has been reported that PDAC takes advantage of its profits by utilising metabolic reprogramming to consume a limited amount of nutrients and to reuse metabolite waste; these abilities indicate that the PDAC cell can adapt to hostile microenvironment by establishing corresponding feedback [26, 27].

1.2.1   Metabolism addiction and metabolic phenotype in PDAC

Similar to the diversity of genomic alterations, PDAC cells are also highly heterogeneous in tumour metabolism. Through broad metabolite profiling, Damen recently reported that PDAC could be classified into three distinct metabolic subtypes: slow proliferating, glycolytic and lipogenic. The glycolytic and lipogenic subgroup differs significantly regarding metabolising glucose and glutamine [28]. Similarly, another study identified four metabolic subtypes: Warburg type, non-canonical type, glucose-dependent mixed type, glutamine-dependent mixed type [29]. Collectively, their findings suggest that

different tumour metabolism may affect tumour destructive behaviour, deter-determining individual phenotypes of PDAC. Likely, the dependency and metabolism of primary nutrients are likely impacted by the dominant oncogenic signalling [30].

1.2.2 Nutrient deprivation in PDAC

By measuring metabolite levels of PDAC, it has been revealed that the microenvironment of PDAC is extremely nutrient poor. Levels of glucose, glutamine and compounds engaging in the tricarboxylic acid (TCA) cycle were dramatically decreased in tumour environment [26]. Potentially, many factors contribute to this severe nutrient deprivation in PDAC. One of them lies in the angiogenesis in that most newly formed vessels are aberrant and non-functional. The abnormal micro-vessels limit nutrient perfusion from blood to tissue, which results in a shortage of nutrient supply [31]. Thus insufficient blood supply contributes to barren microenvironment in PDAC.

Another potential reason causing the nutrient deprivation is the reprogrammed metabolism. Under normoxic conditions, tumour cells tend to use glucose for glycolysis instead of TCA to generate adenosine triphosphate (ATP) and macromolecular. This phenomenon is previously defined as the "Warburg effect". Influenced by Warburg effect, PDAC cells absorb in more glucose from their microenvironment, resulting in reduced glucose levels in their immediate surroundings. As another vital nutrient, glutamine is necessary for maintaining metabolic homoeostasis and TCA cycle replenishment. Despite the fact that tumour cells can scavenge for extracellular protein to acquire glutamine and

other amino acids [26], it does not fulfil the gross requirements, leading to a glutamine-poor microenvironment.

1.3 Cell response under cell-stress conditions

Cancer cells are constantly facing various types of internal or external stress conditions. To survive and adapt in a stressful microenvironment (e.g. above-mentioned nutrient deprivation), cancer cells are capable of initiating a series of biological events to cope with the stressful microenvironment.

1.3.1 Programmed cell death

In normal cells, when stress occurs in the microenvironment, programmed cell death (PCD) is activated to maintain a balance of death and survival. However, in cancer cells, this equilibrium is disturbed. The response to PCD decides cells' ultimate fate [32]. Apoptosis and autophagy are the most common form of PCD.

Apoptosis

Apoptosis is first described by Kerr and colleagues in 1972 [33]. The apoptotic cell changes its structure in two steps: breaking into fragments in the first stage; eliminated and degraded by other cells in the second phase. Three pathways are responsible for triggering apoptosis: intrinsic, extrinsic and intrinsic endoplasmic reticulum pathway [34].

Hypoxia, DNA damage, nutrient deprivation or oxidative stresses initiate the intrinsic pathway, which is tightly regulated by B-cell lymphoma 2 (BCL-2) family members. The extrinsic pathway depends on the transmission of death

signal by death receptors. Tumour necrosis factor (TNF) superfamily plays an active role in mediating signalling transmission and intracellular death domain protein recruitment. Both intrinsic and extrinsic pathways converge to a common pathway mediated by caspase 3. The functional form, cleaved caspase 3, slices the inhibitor of the caspase-activated deoxyribonuclease and initiates nuclear apoptosis [35]. Taken together, cleaved caspase 3 is an important biological marker to determine the apoptotic activity. The third pathway, intrinsic endoplasmic reticulum pathway, is provoked by the unfolded protein accumulation in the endoplasmic reticulum (ER) under stressed condition [36]. However, the underlying mechanisms need to be further investigated.

In PDAC, by either overexpressing proteins of BCL-2 family or blocking death receptor signals, cancer cell acquires apoptosis resistance and escape from cell death [37].

Autophagy

Autophagy is a process through which damaged cytoplasmic organelles and macromolecules are disassembled, allowing for the recycling of major cellular component [38]. Initially, autophagy was classified as a type of cell death-initiating mechanism [39]. Recently, the function of autophagy has been demonstrated to be involved in the carcinogenic process. However, it is controversially discussed whether it is a tumour enhancer or tumour suppressor [40]. On the one hand, autophagy serves as a temporary stress protector for cancer cells under unfavourable conditions such as nutrient deprivation, growth factor shortage, hypoxia and chemotherapy [41]. On the

other hand, autophagy is closely linked with tumour suppression function. As cellular stress accumulates, the persistent activation of autophagy eventually causes cell death. Indeed, the reduced activity in autophagy spontaneously stimulates tumour malignant transformation [42].

In PDAC, the basal autophagy level is higher than that in normal tissue. Coordinated with the liposome function, autophagy is also involved in regulating adaptive metabolic reprogramming [43]. In summary, these data highlights the tumor-promoting role of autophagy in pancreatic carcinogenesis.

1.3.2 Unfolded Protein Response (UPR) and ER stress

ER is a main cellular compartment，in which proteins are modified, assembled, folded and secreted out. Chaperones, foldases, cofactors and processing enzymes form a complex network to ensure an optimized intraluminal environment for protein production [44]. ER homoeostasis is disturbed when unfolded proteins exceed the threshold of folding capacity, resulting in an improper accumulation of unfolded proteins that triggers ER stress. As the consequence of ER stress, cascades of events termed UPR are activated to restore the ER homoeostasis. Three types of sensor proteins -- protein kinase R-like endoplasmic reticulum kinase (PERK), activating transcription factor 6 alpha (ATF6α) and inositol requiring enzyme 1 alpha (IRE1α) -- are responsible for initiating UPR. A 78-kDa glucose-regulated protein (GRP78, also known as BiP) controls UPR activation by supervising these three stress sensor proteins. BiP functions as an ER stress sensor and a master regulator [45].

Many internal and external factors induce ER stress. Under physiologic circumstances, plasma cell differentiation and high glucose-induced pancreatic β-cell dysfunction activate UPR [46]. Under pathologic status, unfavourable living conditions, such as hypoxia, nutrient deprivation, acidosis and chemical damages can also elicit ER stress [47].

Depending on biological contexts, ER stress induction can act as pros or cons. For example, it can promote cell survival while its excessive induction induces cell death [48]. Besides, ER stress has been recently shown to play a role in regulating angiogenesis, metastasis and oncogenic transformation.
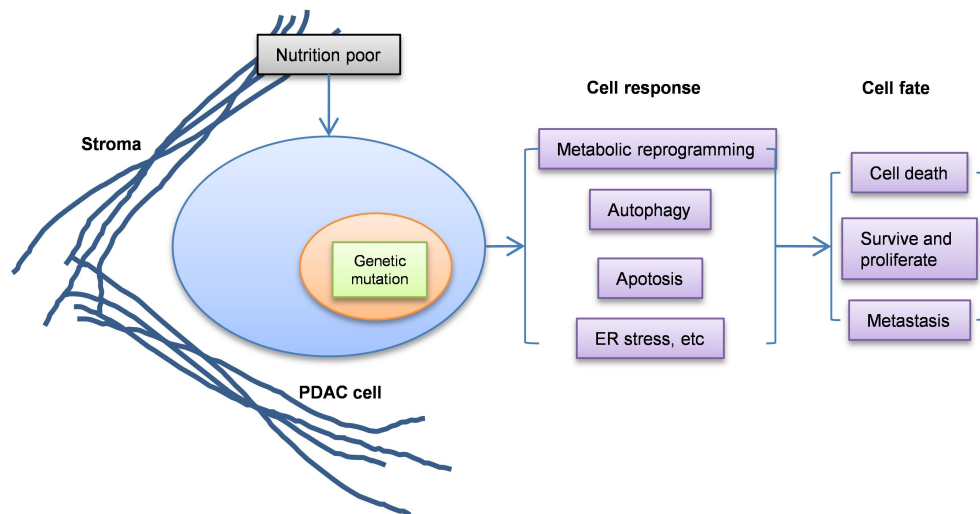
Figure 1. Sketch illustrating PDAC microenvironment and cell response

1.4 Cancer metastasis along with stress-induced cell response

Regardless of a myriad of unfavourable conditions, cancer cells are able to survive in the extremely stressful environment by either evading from current

status or creating appropriately fertile conditions. This adaptation ends up with cancer metastasis as a final consequence.

Cancer metastasis is consisted by four sequent events: 1) invasion and migration; 2) penetration and infiltration into circulation systems; 3) dissemination and extravasation; 4) colonization [49].

The original stress conditions transform tumour cells to a malignant phenotype which are beneficial for metastasizing [50], and during metastasis procedure, the accompanying new stress inhibits or promotes cancer cells to settle down in a target organ [51, 52].

Briefly, unfavourable living conditions, such as hypoxia, nutrient shortage promoting tumour cells to angiogenesis switch [52]. Apoptosis resistance and autophagy favour tumour cells with dysregulated invasion abilities and prolonged survival [53-55]. Activated UPR leaves aberrant ECM components, creates a more spacious environment for tumour cells to move [56]. However, when malignant cells detach from the ECM and begin their 'journey', energy inadequacy caused by floating in a blood vessel can trigger metabolic reprogramming and subsequent response [54, 57]. Although there are many mechanisms co-exist, the dominant one will take the lead and determine cell's fate ultimately [58].
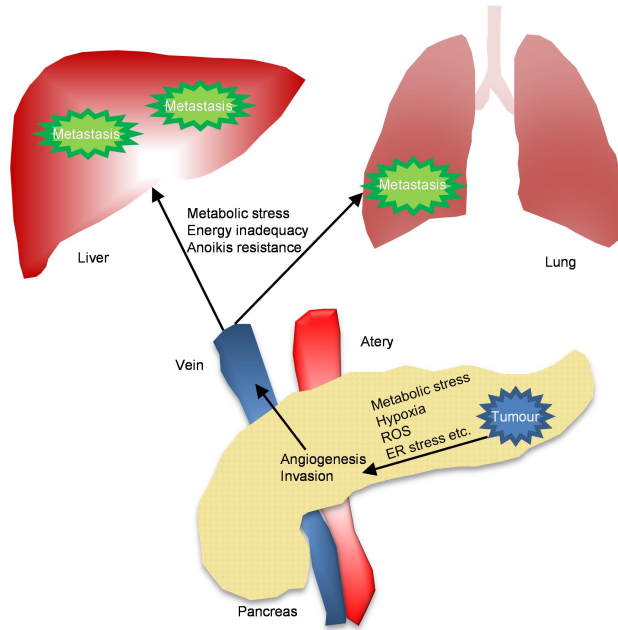
Figure 2. Sketch of PDAC metastasis.

2. AIMS OF THIS STUDY

Due to the acquisition of a number of genetic/epigenetic changes, PDAC cells adapt and survive in the harsh microenvironment with particularly nutrient-limited conditions. Up to now, it is unclear whether the dominant cancer signal may affect the process of such environmental adaption. Furthermore, the biological significance of this phenotypic adaption remains elusive. To this end, we made use of previously characterized murine PDAC cells [59], in which the viability of them rely either on the activity of Mek/Erk or PI3K/Akt to explore the potential link between dominant oncogenic pathways, nutritional reliance and phenotypic changes

Based on existing knowledge and evidence, we hypothesised that:

(1) the dominant pathway may define the reliance of proliferation on specific nutrients;

(2) deprivation of preferred nutrient may induce a number of phenotypic adaption;

(3) adaptive changes may affect malignant behaviours of PDAC.

In particular, we asked the following question:

(1) What is the association between dominant cancer signal and nutritional reliance for cell proliferation?

(2) Are cell lines able to maintain proliferative potential under a nutritionally stressful condition?

(3) How do cancer cells respond to a nutritionally stressful condition *in vitro*, for instance, when the preferred energy source is provided only in a limited concentration?

(4) How does the nutritional adaption alter the tumour histological and biological phenotype *in vivo*?
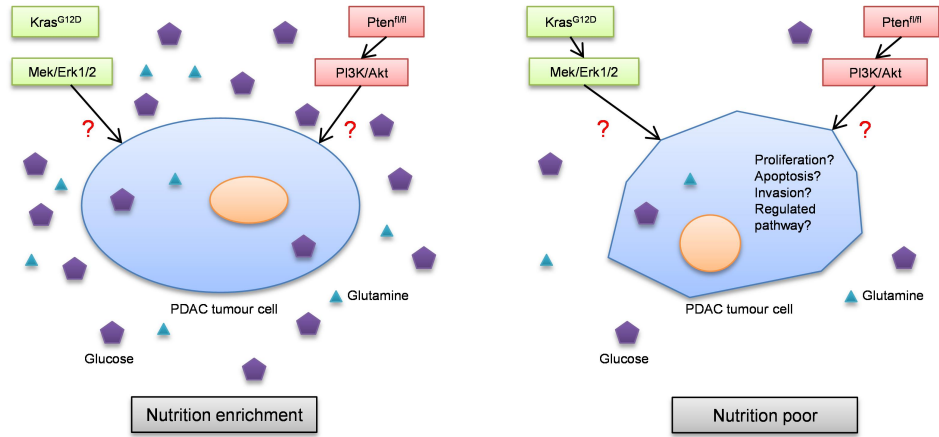
Figure 3. Aim of this study

3. MATERIALS AND METHODS

3.1 Materials

3.1.1 Mouse cell lines

The primary mouse cells 926, and 952 were isolated from genetically engineered mouse model (GEMM) with genotyping as p48$^{Cre/+}$, Pten$^{fl/fl}$, and Tsc1$^{fl/+}$. Cells 399 and 403 were isolated from GEMM with genotyping as p48$^{Cre/+}$, LSL-Kras$^{G12D/+}$, and Tsc1$^{fl/+}$.

3.1.2 Primers

Sequences of primers for QRT-PCR analysis:

Name	Sense (5'→3')	Antisense (5'→3')
Sod1	AACCAGTTGTGTTGTCAGGAC	CCACCATGTTTCTTAGAGTGAGG
Sod2	CAGACCTGCCTTACGACTATGG	CTCGGTGGCGTTGAGATTGTT
Sod3	CCTTCTTGTTCTACGGCTTGC	TCGCCTATCTTCTCAACCAGG
Gpx1	AGTCCACCGTGTATGCCTTCT	GAGACGCGACATTCTCAATGA
Gpx2	GCCTCAAGTATGTCCGACCTG	GGAGAACGGGTCATCATAAGGG
Gpx3	CCTTTTAAGCAGTATGCAGGCA	CAAGCCAAATGGCCCAAGTT
Zep1	GAGGAGGTGACTCGAGCATT	ATTTGTAACGTTATTGCGCCG
Snail1	GACTACCTAGGTCGCTCTGG	GAAGGTGAACTCCACACACG
Cdh1	AACCCAAGCACGTATCAGGG	GAGTGTTGGGGGCATCATCA

Sox9	GCAAGCTGGCAAAGTTGATCT	GCTGCTCAGTTCACCGATG
Vimentin	AACGAGTACCGGAGACAGGT	CAGGGACTCGTTAGTGCCTTT
Kiss1	CTCTGTGTCGCCACCTATGG	TTCCCAGGCATTAACGAGTTC
Spp1	AAGAAGCATCCTTGCTTGGGT	ATGGTCGTAGTTAGTCCTTGGC
Col6a1	CAGCCAGACCATTGACACCA	TTCCTCGCTCCCCCTCATAC
Fn1	ATGTGGACCCCTCCTGATAGT	GCCCAGTGATTTCAGCAAAGG
Ppib	GGAGCGCAATATGAAGGTGC	CTTATCGTTGGCCACGGAGG

3.1.3 List of antibodies

Primary antibodies

Antibody name	Catalogue number	Application*	Producer
Rabbit Anti-PDI mAb[#]	3501	IHC	Cell Signaling Technology (Frankfurt am Main, Germany)
Rabbit Anti-BiP mAb[#]	3177	WB	Cell Signaling Technology
Rabbit Anti-CHOP mAb[#]	5554	WB	Cell Signaling Technology
Rabbit Anti-p-Akt	4060	WB	Cell Signaling Technology

(Ser473) mAb[#]			
Rabbit Anti-p-elF2α (Ser51)) Ab[#]	9721	WB	Cell Signaling Technology
Rabbit Anti-p-Erk1/2 (Thr202/Tyr204) Ab[#]	9101	WB	Cell Signaling Technology
Rabbit Anti-p-mTOR (Ser2448) mAb[#]	5536	WB	Cell Signaling Technology
Rabbit Anti-p-Histone H3 (Ser10) Ab[#]	9701	IHC	Cell Signaling Technology
Rabbit Anti-Cleaved Casp3 mAb[#]	9661 9664	WB IHC	Cell Signaling Technology
Rabbit Anti-LC3B mAb[#]	3868	WB	Cell Signaling Technology
Rabbit Anti-p-AMPKα (Thr172) mAb[#]	2535	WB	Cell Signaling Technology
Rat Anti-Cd31 Ab[#]	DIA-310	IHC	Dianova (Hamburg, Germany)
Rabbit Anti-GAPDH Ab[#]	sc-25778	WB	Santa Cruz Biotechnology (Heidelberg, Germany)
Mouse Anti-β actin Ab[#]	sc-69879	WB	Santa Cruz Biotechnology
Rabbit Anti-SPARC	8725	IHC	Cell Signaling Technology

mAb[#]			
Rabbit Anti-Carbonic Anhydrase IX Ab[#]	ab15086	IHC	Abcam (Cambridge, UK)

Secondary antibodies

Antibody name	Catalogue number	Application*	Producer
Rabbit HRP (horseradish peroxidase)-labelled Anti-Rat IgG Ab[#]	P0450	IHC	Dako (Hamburg, Germany)
Goat HRP-Labelled Polymer Anti-Mouse Ab[#]	K4001	IHC	Dako
Goat HRP-Labelled Polymer Anti-Rabbit Ab[#]	K4003	IHC	Dako
Sheep HRP-labelled Anti-Mouse IgG Ab[#]	NA931	WB	GE Healthcare (Little Chalfont, UK)
Donkey HRP-labelled Anti-Rabbit IgG Ab[#]	NA934	WB	GE Healthcare

[#] Ab=antibody; *Application key: WB = western-blot; IHC = Immunohistochemistry;

3.1.4 Chemicals and Reagents

0.25% trypsin/EDTA	Sigma-Aldrich Chemie GmbH (Munich, Germany)
2-Deoxy-D-glucose	Sigma-Aldrich Chemie GmbH
2-Deoxy-D-glucose 6-phophate sodium salt	Santa Cruz Biotechnology
2-Mercaptoethanol	Sigma-Aldrich Chemie GmbH
β-Nicotinamide adenine dinucleotide phosphate sodium salt hydrate	Sigma-Aldrich Chemie GmbH
Acetic acid	Merck Biosciences (Darmstadt, Germany)
Acetic anhydride	Sigma-Aldrich Chemie GmbH
Acrylamide solution	Carl Roth (Karlsruhe, Germany)
Agarose	Carl Roth
Albumin Fraction V (BSA)	Carl Roth
Ammonium persulfate (APS)	Sigma-Aldrich Chemie GmbH
Biocoat matrigel invasion unit	BD Biosciences (Franklin Lakes, NJ, USA)
Calcium chloride	Carl Roth
Cell lysis buffer (10x)	Cell Signaling Technology
Chloroform	Merck Biosciences

Citric acid monohydrate	Carl Roth
Crystal violet	Carl Roth
Dimethyl sulfoxide	Carl Roth
Diaphorase from Clostridium kluyveri	Sigma-Aldrich Chemie GmbH
Dulbecco's MEM	Sigma-Aldrich Chemie GmbH
DMEM, high glucose, no glutamine	Thermo Fischer Scientific (Dreieich, Germany)
DMEM, no glucose, no glutamine	Thermo Fischer Scientific
D-glucose	Carl Roth
ECL detection reagent	Amersham (Little Chalfont, UK)
Ethanol	Carl Roth
Ethidium bromide	Carl Roth
Ethylenediaminetetraacetic acid disodium salt dihydrate	Carl Roth
Foetal bovine serum	Sigma-Aldrich Chemie GmbH
Formamide	Merck Biosciences
Glucose-6-phosphate Dehydrogenase	Sigma-Aldrich Chemie GmbH

Glycerol	Merck Biosciences
Glycine	Roche Diagnostics (Penzberg, Germany)
Haematoxylin	Merck Biosciences
HEPES	Carl Roth
Hydrochloric acid (5M)	Apotheke TU München (Munich, Germany)
Hydrogen peroxide (30%)	Carl Roth
Histowax	Leica (Wetzlar, Germany)
Isopropanol	Carl Roth
Kaliumchlorid (potassium chloride)	Carl Roth
LDS sample buffer (4x)	Thermo Fischer Scientific
L-Glutamine	Thermo Fischer Scientific
Liquid nitrogen	Tec-Lab (Taunusstein, Germany)
Liquid DAB & chromogen substrate	Dako
Magnesium Sulfate	Sigma-Aldrich Chemie GmbH
Methanol	Merck Biosciences
Molecular weight marker	Fermentas/Termo (Dreieich, Germany)
MOPS	Carl Roth

Dinatrium hydrogenphosphate	Merck Biosciences
Nitrocellulose membranes	GE Healthcare
Normal goat serum	Dako
Nuclear and cytoplasmic extraction reagents	Thermo Fischer Scientific
Para-formaldehyde	Apotheke TU München
Phosphate buffered saline (PBS) pH 7.4	Sigma-Aldrich Chemie GmbH
Polyvinylpyrrolidone	Sigma-Aldrich Chemie GmbH
Permount	Vector Laboratories (Burlingame, CA, USA)
Penicillin-Streptomycin	Sigma-Aldrich Chemie GmbH
Phosphatase inhibitor cocktail	Roche diagnostics
Protease inhibitor cocktail	Roche diagnostics
Proteinase K	Dako
Resazurin sodium salt	Sigma-Aldrich Chemie GmbH
RNAse DNAse-free water	Invitrogen (Karlsruhe, Germany)
Rotiphorese Gel 30 (37,5:1)	Carl Roth
Sample reducing buffer (10x)	Thermo Fischer Scientific
SDS ultra pure	Carl Roth

Sodium borate	Merck Biosciences
Sodium chloride	Carl Roth
Sodium citrate	Merck Biosciences
Sodium hydroxide (5M)	Apotheke TU München
Sodium phosphate	Merck Biosciences
TEMED	Carl Roth
Tetraethylammonium chloride	Sigma-Aldrich Chemie GmbH
Thiazolyl Blue Tetrazolium Bromide (MTT)	Sigma-Aldrich Chemie GmbH
Triethanolamine	Sigma-Aldrich Chemie GmbH
Tris base	Sigma-Aldrich Chemie GmbH
Triton X 100	Carl Roth
Trypan blue solution	Sigma-Aldrich Chemie GmbH
Tween 20	Carl Roth
PBS powder without Ca^{2+}, Mg^{2+}	Biochrom AG (Berlin, Germany)

3.1.5 Kits

ADP/ATP Ratio Assay Kit	Bioassay Systems (Hayward, America)

BCA Protein Assay Kit	Thermo Fischer Scientific
Glutamate Assay Kit	Abcam
Mouse Extracellular Matrix&Adhesion Molecular RT^2 Profiler PCR Array	Qiagen (Hilden, Germany)
NADP/NADPH Assay Kit	Abcam
Qproteome Cell Compartment Kit	Qiagen
QuantiTect Rev. Transcription Kit	Qiagen
Mouse VEGF Quantikine ELISA Kit (MMV00)	R&D Systems (Wiesbaden, Germany)
RNeasy Mini Kit	Qiagen
SYBR Green 1 Master Kit	Roche Diagnostics

3.1.6 Buffers and Solutions

Immunohistochemistry

10x Tris Buffered Saline (TBS)

Tris base	12.1 g
NaCl	85 g
Distilled Water	800 ml
Adjust pH to 7.4 with	5 M HCl

Constant volume with distilled water	to 1000 ml

20x Citrate buffer

Citric acid (Monohydrate)	21.0 g
Distilled water	300 ml
Adjust to pH 6.0 with	5 M NaOH
Constant volume with distilled water	to 500 ml

Washing Buffer (1xTBS+0.1%BSA)

10xTBS	100 ml
BSA	1 g
Constant volume with distilled water	to 1000 ml

Western Blott

Electrophoresis buffer

MOPS	209.2 g
Tris Base	121.2 g
SDS	20 g
EDTA-free acid	6 g
Constant volume with distilled water	to 1 l

Transfer Buffer

Tris base	29.1 g
Glycine	14.7 g
Methanol	1000 ml
SDS	0.1875 g
Constant volume with distilled water	to 5 l

Washing buffer

10xTBS	100 ml
Tween 20	0.5 ml
Constant volume with distilled water	to 1000 ml

Blocking Buffer

Dry milk or BSA	0.5 g
Washing buffer	10 ml

Glucose uptake

KRH (Krebs-Ringer-HEPES) buffer

HEPES	50 mM
NaCl	137 mM
KCl	4.7 mM

CaCl$_2$	1.85 mM
MgSO$_4$	1.3 mM
BSA	0.1% (w/v)
Adjust to pH 7.4 with	0.5 M NaOH

TEA (triethanolamine) buffer, 200 mM

TEA	200 mM
Adjust to pH 8.1 with	1 M NaOH
Constant volume with distilled water	to 50 ml

Assay solution

200 mM TEA	2.5 ml
0.4% BSA	500 µl
10 mM NADP	100 µl
Diaphorase	2 units
2 mM Resazurin sodium salt	10 µl
L mesenteriodes G6PDH	150 units
Constant volume with distilled water	to 10 ml

3.1.7 Laboratory equipment

Analytic balance	Mettler (Giessen, Germany)
Balance	Scaltec (Göttingen, Germany)
Biophotometer	Eppendorf (Hamburg, Germany)
Centrifuge	Eppendorf
CO_2 incubator	Sanyo (Secausus, NJ, USA)
Computer Hardware	Fujitsu SIEMENS (Tokyo, Japan)
Electrophresis/Electroblotting equipment/ power supply	Invitrogen
Freezer -20°C	Liebherr (Bulle, Switzerland)
Freezer -80°C	Heraeus (Hanau, Germany)
Fluorescence reader	Promega
Luminescence reader	Promega
Microplate reader	Thermo Fischer Scientific (Dreieich, Germany)
Microscope	Leicca (Wetzlar, Germany)
Microwave oven	Siemens (Munich, Germany)
PH-meter	Bechman (Washington, DC, USA)
Power supply	Biometra (Göttingen, Germany)

Refrigerator 4°C	Comfort (Buller, Switzerland)
Roche LightCycler 480	Roche
Roller mixer	Stuart (Stone, UK)
Scanner	Canon (Tokyo, Japan)
Spectrophotometer	Thermo Fischer Scientific (Dreieich, Germany)
Sterilgard Hood	Thermo Fischer Scientific (Dreieich, Germany)
Thermomixer	Eppendorf
Vortex Mixer	Neolab (Heidelberg, Germany)
Water bath	Lauda (Lauda-Koenigshofen, Germany)
Stereomicroscope	Zeiss
Tissue embedding machine	Leica (Wetzlar, Germany)
Tissue processor	Leica
Glucose meter (Precision Xceed)	Abbott GmbH (Wiesbaden, Germany)

3.1.8. Consumables

Blotting paper	Whatman (Maidstone, Kent, UK)
Cell scraper	Sarstedt (Nuembrecht, Germany)

Coverslips	Menzel (Braunschweig, Germany)
Filter (0.2 µm)	Neolab (Heidelberg, Germany)
Filtertip (10 µl, 20 µl, 100 µl, 200 µl, 1000 µl)	Starlab
Hyperfilm	GE Healthcare (Little Chalfont, UK)
Pure nitrocellulose membrane (0.45 µM)	Bio-rad
Sterile needles	BD (Franklin Lakes, NJ, USA)
Tissue culture dishes (60x15 mm; 100x20 mm)	Sarstedt (Nuembrecht, Germany)
Tissue culture flasks (25 cm^2; 75 cm^2; 125 cm^2)	Greiner Bio-one (Frickenhausen, Germany)
Tissue culture plates (6-well; 24-well; 96-well)	Greiner Bio-one
Ultra-Low attachment multiwell plates (24-well)	Sigma
Ultra-Low attachment cell culture flasks (25 cm^2)	Sigma
Tubes (15 ml; 50 ml)	Greiner Bio-one

3.2 Methods

3.2.1 Cell culture

Control cells were held culturing in normal DMEM (Sigma-Aldrich) supplemented with 10% foetal bovine serum (FBS), 100 u/ml of penicillin, and 100 µg/ml of streptomycin at 37ºC, 5% CO_2. A low-glucose conditional medium was prepared from glucose-free DMEM (Thermo Fischer Scientific) supplemented with 0.5 mM of D-(+)-glucose (Carl Roth), 10% FBS, 100 u/ml of penicillin, and 100 µg/ml of streptomycin. A low-glutamine conditional medium was prepared from glucose and glutamine-free DMEM (Thermo Fischer Scientific) supplemented with 25 mM of D-(+)-glucose, 1 mM of L-glutamine (Thermo Fisher Scientific), 10% FBS, 100 u/ml of penicillin, and 100 µg/ml of streptomycin. A low-glucose and low-glutamine conditional medium was prepared from glucose and glutamine-free DMEM supplemented with 0.5 mM of D-(+)-glucose, 1 mM of L-glutamine, 10% FBS, 100 u/ml of penicillin, and 100 µg/ml of streptomycin. For selection treatment, the cells were split into two 10 cm petri-dishes, cultured with either a normal medium or a nutrient-deprivation medium. After 30 days of culture, surviving clones or cells were collected for further use. Before experimentation, the selected control or nutrient-deprivation cells were grown back in a normal DMEM medium for 48 hours or for a longer time.

3.2.2 Immunohistochemistry analysis

The paraffin-embedded full tissue was consecutively cut into 3-µm thick sections, then deparaffinized and rehydrated. Antigen retrieval was carried out with a citrate buffer (pH 6.0; 10 mM citric acid, 0.05% Tween-20) in a

microwave oven for 12-15 minutes. After cooling down, 3% hydrogen peroxide diluted in 100% methanol was used to block endogenous peroxidase. Next, a 3% bovine serum albumin (BSA) or a goat serum was applied to prevent non-specific binding. The sections were incubated respectively with anti-cleaved Caspase-3 Cell Signaling Technology) at 1.25 µl/ml, anti-phospho-Histone H3 (Cell Signaling Technology) at 2 µl/ml, anti-CD31 (Dianova) at 4 µg/ml, anti-Bip (Cell Signaling Technology) at 3.33 µl/ml, and anti-Sparc (Cell Signaling Technology) at 10 µl/ml at 4ºC overnight. Then, an anti-mouse (Dako), anti-rabbit (Dako), or polyclonal rabbit anti-rat second antibodies (Dako) were applied on the section, and a Liquid DAB+ Substrate Chromogen System (Dako) was used for the colour reaction. After counterstaining with Mayer's hematoxylin, the slides were dehydrated and mounted.

3.2.3 mRNA and cDNA preparation

Following the manufacturer instructions of the RNA extraction kit (Qiagen), mRNA from the murine PDAC cell line was extracted. cDNA transcription was conducted according to the manufacturer's instructions of the cDNA transcription kit (Qiagen).

3.2.4 Quantitative Real-Time Chain Reaction

A quantitative real-time PCR (QRT-PCR) was performed with the LightCycler^{TM}480 system using the SYBR Green 1 Master Kit (Roche Diagnostics). Target gene expression was normalized to the mouse housekeeping gene PpiB (Peptidylprolyl Isomerase B) with the LightCycler^{TM}480 software (Roche Diagnostics).

3.2.5 Immunoblot analysis

Protein extraction from cells:

Before protein extraction, the cells were washed twice with ice-cold PBS (pH 7.4; 0.01 M PBS). The 10x cell lysis buffer (Cell Signaling Technology) was diluted with distilled water to one fold and added with the protease inhibitor (Roch diagnostics) and the phosphatase inhibitor (Roche Diagnostics). After adding the ice-cold cell lysis buffer for 30 minutes, the cells were immediately homogenised with an ultrasound wave for 15 seconds and centrifuged at 14,000 g at 4ºC for 15 minutes. The supernatant was kept, and the protein concentration was measured with a BCA Protein Assay kit (Thermo Fischer Scientific), following the manufacturer's instructions.

Western blotting:

Roughly 20 µg of the total proteins were loaded, separated in 7.5%-10% SDS-PAGE, and then transferred to a PVDF membrane (Bio-rad). The membrane was blocked for one hour using either 5% dry milk or 5% BSA diluted in 0.05% Tween-20-TBS. Afterwards, the membrane was incubated initially with the first antibodies at 4ºC overnight. Before secondary antibody incubation, the membrane was washed with 0.05% Tween-20-TBS for three times. A secondary antibody was used at room temperature. Afterwards, band signals were detected with an Amersham Hyperfilm ECL film (GE Healthcare).

3.2.6 Mouse Vegfa Elisa measurement

Various kinds of cell lines were trypsinized, counted, and seeded with the normal culture medium in six-well plates. Afterwards, the cells were washed

with PBS and incubated with 1 ml of an FBS-free medium under standard conditions for 24 hours. Afterwards, the supernatants were collected, and the Vegfa concentration was measured according to the manufacturer's instructions of the commercial mouse VEGF quantikine ELISA Kit (R&D Systems).

3.2.7 RT^2 PCR Array

Reagents and material for the RT^2 Profiler^{TM} PCR array were obtained from Qiagen. The assay was performed according to the manufacturer's instructions of the mouse extracellular matrix and the adhesion molecules arrays kit (Qiagen). Data were analysed using the web-based software from Qiagen: (www.sabiosciences.com/pcr/arrayanalysis.php). Group-wise comparisons were performed using a Student's *t*-test.

3.2.8 Colony formation assay

Cells were trypsinized and counted in logarithmic phase. In a single well of the six-well plate, $3×10^2$ cells were seeded. The next day, adherent cells were washed with PBS and incubated with conditioned medium (0.5 mM of D-glucose medium or 1 mM of L-glutamine medium) for seven days of culture. Then, the formed colonies were fixed with a mixture of 75% methanol and 25% acetone, stained with 10% crystal violet, and counted individually by two different researchers.

3.2.9 MTT assay

For evaluation of cell proliferation after the nutrient-deprivation treatment, control or selected cells were seeded with a normal, complete DMEM medium at 2,000 cells per 100 µl in 96-well plates. After 24, 48, 72, and 96 hours, 50 µg of Thiazolyl blue tetrazolium bromide (MTT, Sigma-Aldrich) was added to each well and kept for four hours. Then, the supernatant was discarded, and 100 µl of 2-propanol (Carl Roth, Karlsruhe, Germany) was added to each well. The absorbance values were determined at 570 nm.

3.2.10 Invasion assay

Cell invasion assay was carried out using a transwell chamber (Thermo Fischer Scientific) to evaluate murine tumour cell migration and invasion abilities. Briefly, after trypsinizing, both the nutrient-deprivation selected cells and the control cells (2×10^4/ml) were resuspended in 200 µl of the FBS-free medium in the upper chamber and 500 µl of a normal DMEM medium (10% FBS) was added to the lower chamber. The whole chamber was cultured under standard condition (37°C, 5% CO_2) for 24 hours. Afterwards, the chamber membrane was fixed with 100% methanol and stained with 10% crystal violet. The total invaded cell numbers were counted under a microscope.

3.2.11 Cell transplantation experiment

For the orthotopic xenograft mouse models, selected low-glucose murine PDAC tumour cells or control cells (1×10^6) were trypsinized, resuspended in 50 µl of PBS, and injected into the pancreatic tails of eight-week-old C57BL/6J mice. After four weeks, the experimental mice were sacrificed, and the pancreatic tumours were collected. For the portal vein injection mouse models,

$5x10^5$ of low-glucose selected or control cells were counted, resuspended in PBS, and inoculated into the portal vein of the C57BL/6J mouse. After two weeks, the experimental mice were sacrificed, and the entire liver lobes were collected. For the tail-vein injection mouse models, $1x10^6$ of tumour cells were resuspended in 150 μl of PBS and injected slowly into the tail vein. The mice were kept for three weeks before 18F-FDG PET. Afterwards, both sides of pulmonary lobes were collected for later experiments. All studies were performed under the agreement of a protocol approved by the Animal Care and Use Committee of the Technical University of Munich (ethical application approval no. 42-13).

3.2.12 Microarray Experiment and data analysis

Triplicate samples of the control cells and the low-glucose selected cells were analysed by using Affymetrix GeneChip Mouse Gene 1.0 ST microarrays according to the manufacturer's instructions. Normalization was performed according to the Robust Multichip Average (RMA) method. Low-expression or small variation genes were discarded with the nsFilter method. A linear model and a one-way ANOVA were used for identifying differentially expressed genes. Those differentially expressed genes involved in angiogenesis and the regulation of angiogenesis was determined through gene ontology analysis and KEGG analysis.

3.2.13 Glucose uptake assay

Glucose uptake was measured following the detailed instructions published by Yamamoto and co-authors [60]. Briefly, 10^5 cells were seeded in one well of a 24-well plate. After overnight incubation, the adherent cells were washed with

a washing buffer and incubated with 2 mM of 2-deoxy-D-glucose (Sig-(Sigma-Aldrich) under culture conditions for 20 minutes. The cells' 2-deoxy-glucose-6-phosphate (DG6P) concentrations were measured using a fluorescence reader, calculated according to a standard curve, and normalised against the total cell number.

3.2.14 Glutamate assay

A 10^6-cell suspension was collected and washed with ice-cold PBS. The cell suspension was dissolved in assay buffer provided in the Glutamate Assay Kit (Abcam). Afterwards, the sample was transferred into a 96-well plate for colour reaction. The glutamate level was measured at 450 nm, and calculated according to a standard curve.

3.2.15 ADP, ATP, and ADP/ATP ratio measurement

Measurements of ADP, ATP, and ADP/ATP ratios were performed following the manufacturer's instructions of the EnzyLight™ ADP/ATP Ratio Assay Kit (BioAssay Systems). Briefly, 10^4 cells were counted and seeded in a white, opaque microplate. After adherence, the culture medium was discarded, and the ATP/ADP reagent was added separately to cells. A luminometer (Promega) obtained the OD values, ATP and ADP amounts were measured according to a standard curve. The ADP/ATP ratio was calculated accordingly.

3.2.16 Anoikis assay

A 500-µl cell suspension containing $1×10^4$ cells was seeded in an anchorage-resistant plate (Sigma-Aldrich). The cells were cultured under

standard conditions for 48 hours before supplemented with 50 µL of 250-µg MTT. Afterwards, the cells were incubated for four hours at 37ºC before 500 µL of cell lysis buffer (10% SDS, 0.01 M HCl) was added in. The mixture was kept culturing in the dark for 24 hours. After incubation, the 200-µL mixture was transferred into a 96-well plate, and the absorbance value was measured at 570 nm.

3.2.17 Liver metastasis area analysis

After morphological examination, the slides were scanned with a 1.25× object by using a Zeiss microscope. ImageJ (1.48v) and   Matlab (R2015a) was used for counting the tumour's metastasis area and total liver area separately. The metastasis area ratio was calculated as follows:

$$\text{ratio} = \frac{\text{metastasis area in (median + left + right + caudate) lobe}}{\text{total area (median + left + right + caudate) lobe}} \times 100\%$$

3.2.18 Patients' tissue-collection and necrosis area analyses

The PDAC patients' tissue were collected, fixed in paraformaldehyde, and embedded in paraffin The use of the patient material was approved by the patients before surgery as well as by the local ethics committee (Department of Surgery, Klinikum Rechts der Isar, Technical University Munich). Carsten Jäger coordinated tissue collection and patient database maintenance. A necrosis-area analysis was performed from PDAC patients with or without diabetes. Two independent researchers scanned the complete section of each PDAC patient's H&E staining and classified it into either the necrosis group or

the non-necrosis group. Afterwards, the necrosis ratio of each patient was calculated, and the Chi-square test was performed to obtain the p value.

3.2.19. Statistical analysis

Statistical analysis was performed by GraphPad Prism 6 (GraphPad) or IBM SPSS 22 Software (Statistical Package for the Social Sciences). The Fisher's exact test was conducted to compare the distribution of categorical factors of different groups. All experiments were performed independently at least three times. Unless otherwise stated, an unpaired Student's t-test was used for group-wise comparisons of two groups. The data significance level was set at $p < 0.05$. Results are expressed as a mean ± standard error of the mean (SEM) unless indicated otherwise.

4. RESULTS

4.1 Mek/Erk-dependent PDAC cells rely on glucose while PI3K/Akt-dependent PDAC cells depend on glutamine for proliferation

To test whether the dominant oncogenic pathway affect environmental adaption for cell proliferation, we performed the colony-formation assay using a number of previously characterized Mek/Erk-dependent and PI3K/Akt-dependent murine PDAC cell lines [59]. This analysis revealed that Mek/Erk-dependent cells relied more on glucose for proliferation than others. Under the glucose-free condition, the formed colony number decreased by 80% in Mek/Erk-dependent cells, while it diminished by only 10% to 50% in the other two types of cells (Figure 4). Meanwhile, the high proliferation level of 926, 952, and 975 cells in a glucose-free medium indicated that Akt activation might facilitate PI3K/Akt-dependent cells with other nutrient supply. This phenomenon suggested that glucose was not a requisite nutritional source for PI3K/Akt-dependent cells.
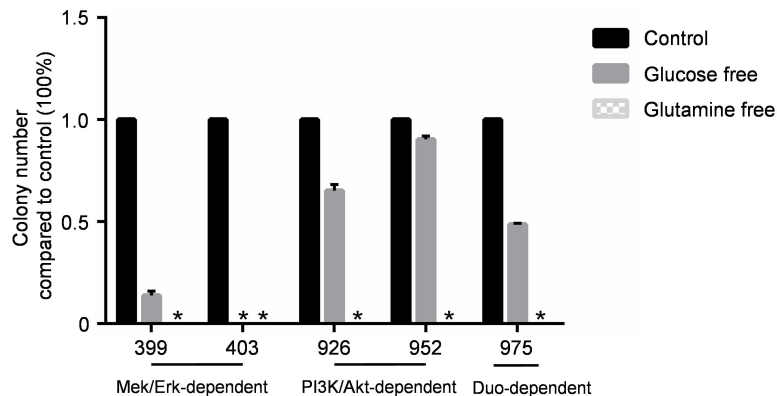
Figure 4. Colony formation result shows Mek/Erk-dependent cells rely on glucose for proliferation; PI3K/Akt-dependent cells do not rely on glucose for proliferation. The data are represented as mean ± SEM (n = 3).

To examine the lowest glucose or glutamine concentration at which murine tumour cells could proliferate, a colony-formation assay was performed using a Mek/Erk-dependent cell line - 399 and PI3K/Akt-dependent cell line - 926. Various concentrations of glucose or glutamine were provided separately to 399 and 926 cells. After seven days of culture in the nutrient limited environments, formed colonies were counted to evaluate cell survival and proliferation. The result showed that 0.5 mM of glucose and 1 mM of glutamine were the minimal amounts of nutrients to maintain 399 and 926 proliferation. Thus, these two concentrations were chosen for the following experiments.
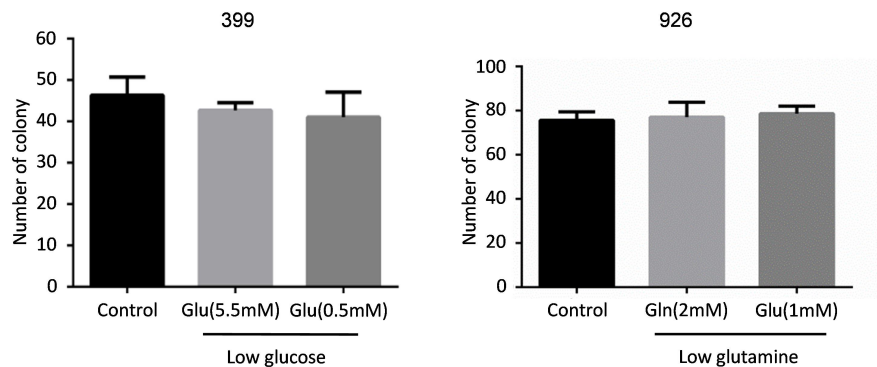
Figure 5. Colony-formation assay shows Mek/Erk-dependent cells (left panel), and PI3K/Akt-dependent (right panel) cells maintain proliferation under nutrient –limited culture condition. Data is derived from three independent experiments. Glu: glucose; Gln: glutamine.

Due to the highly proliferative features and fast expansion, PDAC tumour cells are always exposed to a relatively nutrient-limited microenvironment. With neovascularization, tumour cells return to a nutrient-rich environment again [61, 62]. To determine the influence of oncogene addiction and nutrient fluctuation

on murine PDAC cells, we first cultured tumour cells in a microenvironment with minimal amounts of glucose or glutamine for 30 days. Then, we cultured the adaptive cells back to normal nutrient conditions for 48 hours to mimic glucose or glutamine fluctuation cycle.
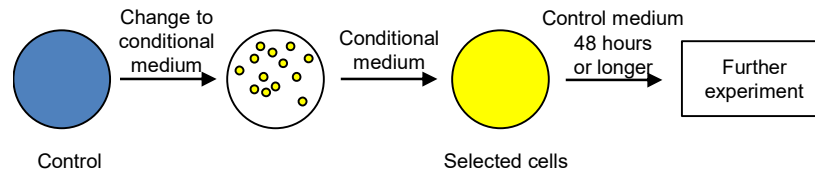

Figure 6. Scheme view of the experimental setup. The blue colour represents untreated control cells, and the yellow colour signifies the selected low-glucose cells. All experiments, unless specifically highlighted, are performed after the selected cells are returned to a normal medium for 48 hours.

Table 1. Conditional medium formula

Medium	Glucose Concentration (mM)	Glutamine Concentration (mM)
Control	25	4
Low glu	0.5	4
Low gln	25	1
Low glu & gln	0.5	1

Table 1. Essential nutrient concentration in the conditional medium. glu: glucose; gln: glutamine

4.2 The Mek/Erk-dependent cell line is conservative while the PI3K/Akt-dependent cell line is sensitive to a nutrient-limited environment

In order to adapt to the nutrient fluctuation microenvironment, PDAC cells needed to adjust the internal biological programme. Thus we examined if the oncogenic phenotype was maintained after limited nutrient selection. The western blot result showed that the phosphorylation of Erk1/2$^{Thr202/Tyr204}$ was

barely influenced by both cell types. In Mek/Erk-dependent cells - 399, the Akt^{Ser473} phosphorylation remained same as the counterpart; however, in the PI3K/Akt-dependent cells - 926, Akt phosphorylation at Ser473 site was impaired in all three nutrient limited groups (Figure 7). This indicates that PI3K/Akt-dependent cells were more sensitive to nutrient deprivation.
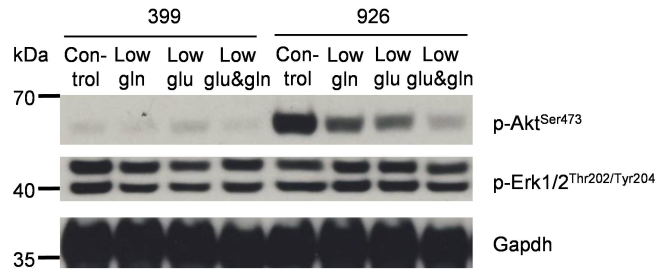

Figure 7. The western blot result shows no obvious difference of pospho-Akt^{Ser473} and phospho-Erk1/2$^{Thr202/Tyr204}$ among the subgroups of Mek/Erk-dependent cell line 399; however, the expression of pospho-Akt^{Ser473} was impaired in nutrient-limited groups of PI3K/Akt-dependent cell line 926, demonstrating Mek/Erk-dependent cell line 399 maintains intrinsic oncogenic phenotype, while phosphorylation of Akt^{Ser473} is inhibited in PI3K/Akt-dependent cell line 926 after nutrient deprivation selection.

4.3 Proliferation state assessment after nutrient deprivation selection

Since proliferation ability is an important indicator to determine cell behaviour, we first investigated the proliferation capacity of the adapted and the control cells. MTT optical density value and proliferation tendency were similar among nutrient-limited group and control group (Figure 8), which confirmed that nutrient alteration in tumour microenvironment did not affect PDAC cell proliferation ability.
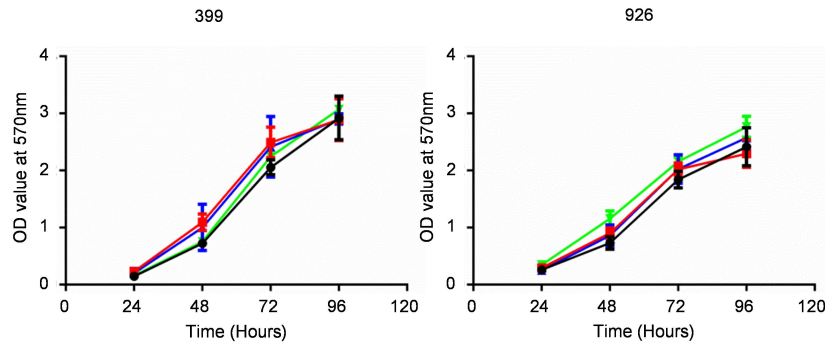
Figure 8. The MTT assay shows proliferation ability was not affected by nutrient deprivation selection in Mek/Erk-dependent cell line 399 (left panel) and PI3K/Akt-dependent cell line 926 (right panel) from 24 hours to 96 hours. Data are shown from three replicates.

4.4 Metabolic state assessment after nutrient deprivation selection

4.4.1 The Mek/Erk-dependent cell line increases glucose uptake

Glucose uptake and glutamine assays were carried out. In PI3K/Akt-dependent cells (926), the glucose uptake and intracellular glutamine level remained similar between experimental and control groups (Figure 9a, 9b). In Mek/Erk-dependent cells (399), intracellular glutamine level was not affected by nutrient-deprivation selection, but G6P accumulation in the selected low-glucose cells was 2-fold higher than that in control cells (p = 0.0124, Figure 9a).
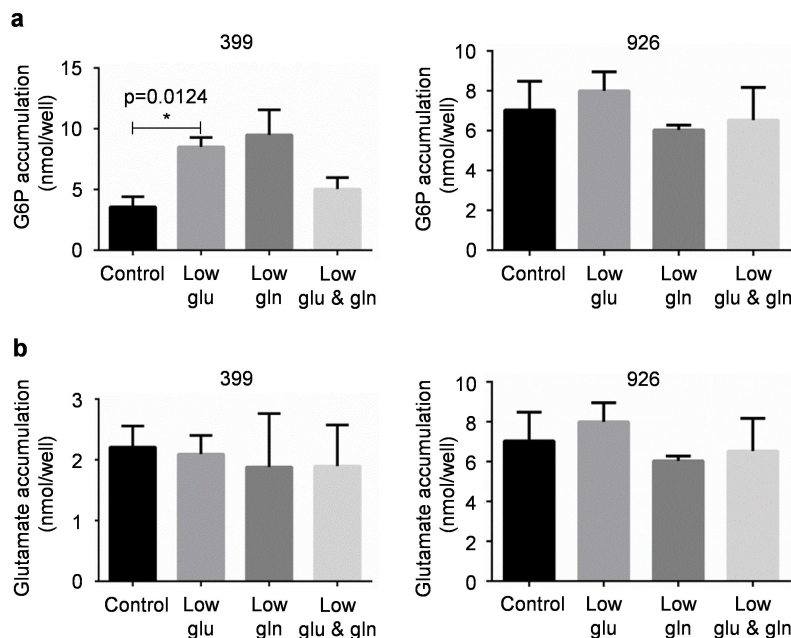
Figure 9. (a) Glucose uptake experiment shows elevated glucose uptake in the low-glucose group of Mek/Erk-dependent cell 399 (left panel) while no differences in PI3K/Akt-dependent cell 926 (right panel). **(b)** Intracellular glutamate assay shows no differences among subgroups of both 399 (left panel) and 926 (right panel) cell line. Data are expressed as a mean ± SEM and obtained from triple replicates. Statistical significance is determined by an unpaired t-test, *: $p < 0.05$.

4.4.2 the PI3K/Akt-dependent cell line increases reactive oxygen species (ROS) elimination related gene expression

Under physiological circumstances, ROS production and elimination are regulated by the scavenging system and maintained at a stable level. In cancer cells, abnormal ERK signalling [63, 64] or AKT signalling [65, 66] pathway activation leads to the accumulation of intracellular ROS levels. Enzymatic antioxidants, including superoxide dismutase (SOD) and glutathione peroxides (GPX), catalyse intracellular ROS to oxygen and water [67]. Accordingly, we examined the mRNA expression level of these functional genes. In Mek/Erk-dependent cells 399, no significant difference was observed in the tested genes (Figure 10a). In PI3K/Akt-dependent cells-926, the

glutamine-deprivation group demonstrated higher Sod1, Sod2 and Gpx1 mRNA expression level (Figure 10b). This data indicated an efficient ROS elimination response took place in PI3K-Akt dependent cells cultured under nutrient-limited microenvironment.
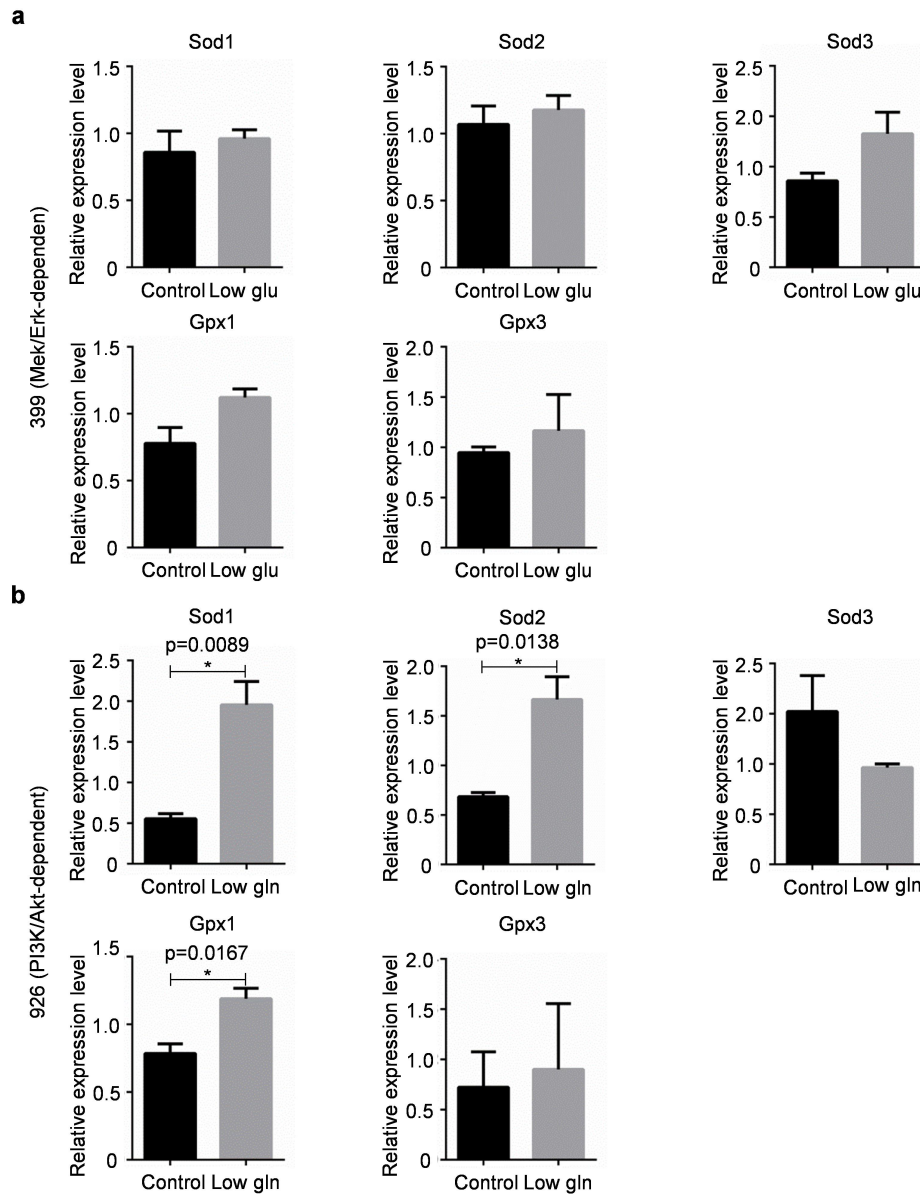

Figure 10. (a) The Mek/Erk-dependent cell line shows no significant mRNA level differences in ROS enzyme gene. **(b)** The PI3K/Akt-dependent cell line catalyses more ROS into the water in the nutrient limited group cells. All results

are presented as the means ± SEM of triplicate experiments, statistical signif-significance is determined by an unpaired *t*-test, *: $p < 0.05$.

4.4.3 Both the Mek/Erk-dependent and the PI3K/Akt-dependent cells show elevated ATP production and consumption

Energy generation and the ADP/ATP ratio reflect an overall metabolic status in tumour cells. Thus, we examined intracellular ATP production and consumption status after nutrient-fluctuation treatment.

Interestingly, Mek/Erk-dependent and PI3K/Akt-dependent cells shared a common feature in the nutrient-limited group. Both cell lines elevated ATP and ADP production. Though the ADP/ATP ratio was not affected (Figures 11a and 11b).
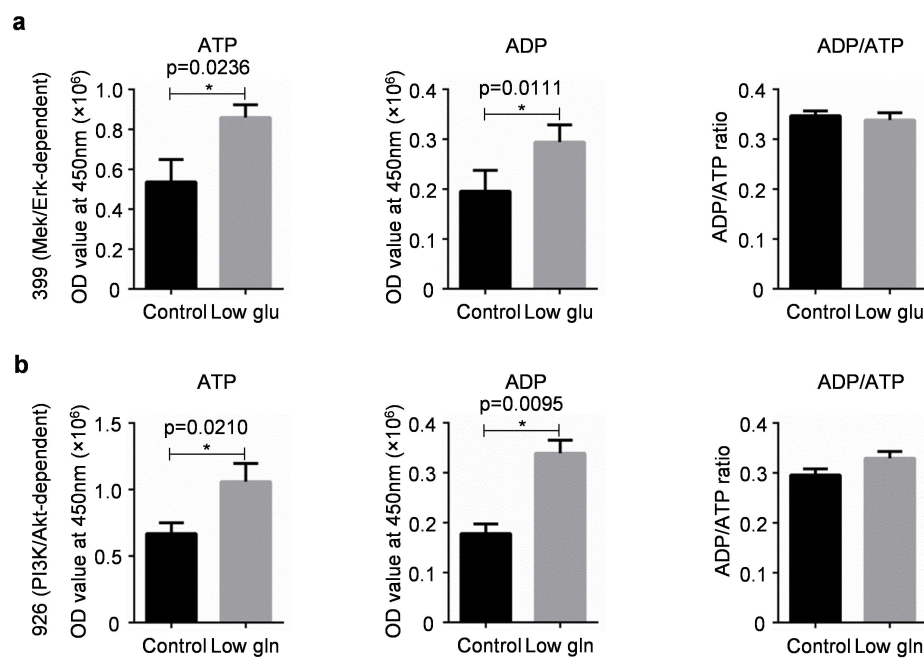
Figure 11. (a) Mek/Erk-dependent cells show higher intracellular ATP (left panel), and ADP (middle panel), but no differences in ADP/ATP ratio (right panel) **(b)** PI3K/Akt-dependent cells shows similar. The values are from triplicate independent experiments, expressed as mean ± SEM, where the *p* value is from an unpaired *t*-test ($p <0.05$).

4.5 Functional assays after nutrient deprivation selection

4.5.1 Nutrient deprivation promote invasive potentials in adaptive cells in both Mek/Erk-dependent and PI3K/Akt-dependent cells

We conducted an invasion assay to determine invasive potentials after the nutrient physiological selection process. Regarding Mek/Erk-dependent cells, only the clones adapted in low-glucose environment exhibited a higher invasion capacity. As for PI3K/Akt-dependent cells, the clones that survived and proliferated in glutamine-limited conditions showed increased invasive potentials (Figure 12a). To eliminate the differentiation caused by clone diversity, these experiments were also reproduced in other cell lines [59]. Similarly, only glucose-deprivation conditions select invasive Mek/Erk-dependent cells. Regardless of glucose conditions, only glutamine-deprivation environments select invasive PI3K/Akt-dependent cells (Figure 12b).
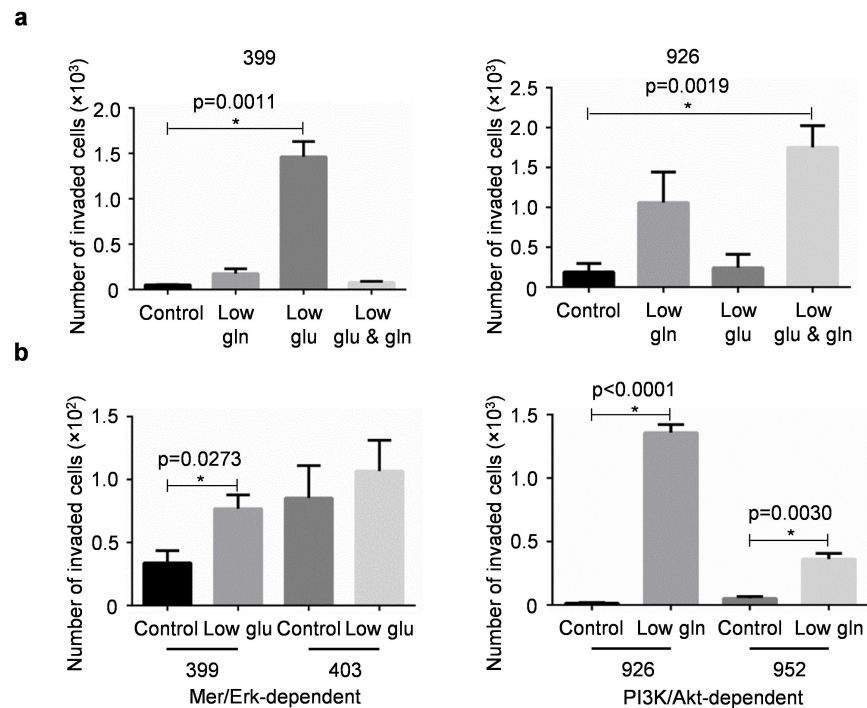
Figure 12. (a) Invasion assay on adaptive clones shows that low-glucose culture condition selects invasive clones in Mek/Erk-dependent cells (left

panel), while low-glutamine culture conditions select invasive cells in PI3K/Akt-dependent cells (right panel). **(b)** Invasion assay reproduced using other cells with the similar genetic background; all data are presented as a mean ± SEM; the *p* value is from an unpaired *t*-test, *: $p < 0.05$.

4.5.2 Mechanistic exploration of increased invasive potentials

PDAC cells are usually accompanied with apoptosis resistance, autophagy activation, and epithelial mesenchymal transition (EMT) [68, 69]. These characteristics may potentially contribute to the invasive and metastatic phenotype.

4.5.2.1 EMT is involved in increased invasive potentials

EMT is associated with increased invasive potentials in PDAC [70]. During EMT process, tumour cells lose epithelial markers, transform to a mesenchymal phenotype, acquire invasion abilities, and gain stem cell properties [71-74]. The whole process is featured by decreasing epithelial marker expression (e.g. E-cadherin) but increasing mesenchymal marker expression (e.g. Vimentin, N-cadherin). Transcription factors (e.g. Sox9, Snail, Zeb1, Zeb2, Slug, and Kiss1) also play important roles [75-77].

The mRNA expression level of Zeb1 was up-regulated in both adaptive cells (399 and 926, Figures 12a and 12g), while the expressions of Snail, Sox9, and Kiss1 were differently regulated. The adaptive 399 cells showed increased expression of Snail, Kiss1, but down-regulation of Sox9 (Figures 12b-d); In comparison, 926 cells showed down-regulation of Snail, Kiss1, but up-regulation of Sox9 (Figures 12h-j). In 399 cells, neither E-cadherin nor Vimentin was differently expressed (Figures 12e and 12f). In 926 cells, the E-cadherin expression level was significantly (3-fold) higher in adaptive cells than that in parental cells ($p = 0.0003$, Figure 12k).
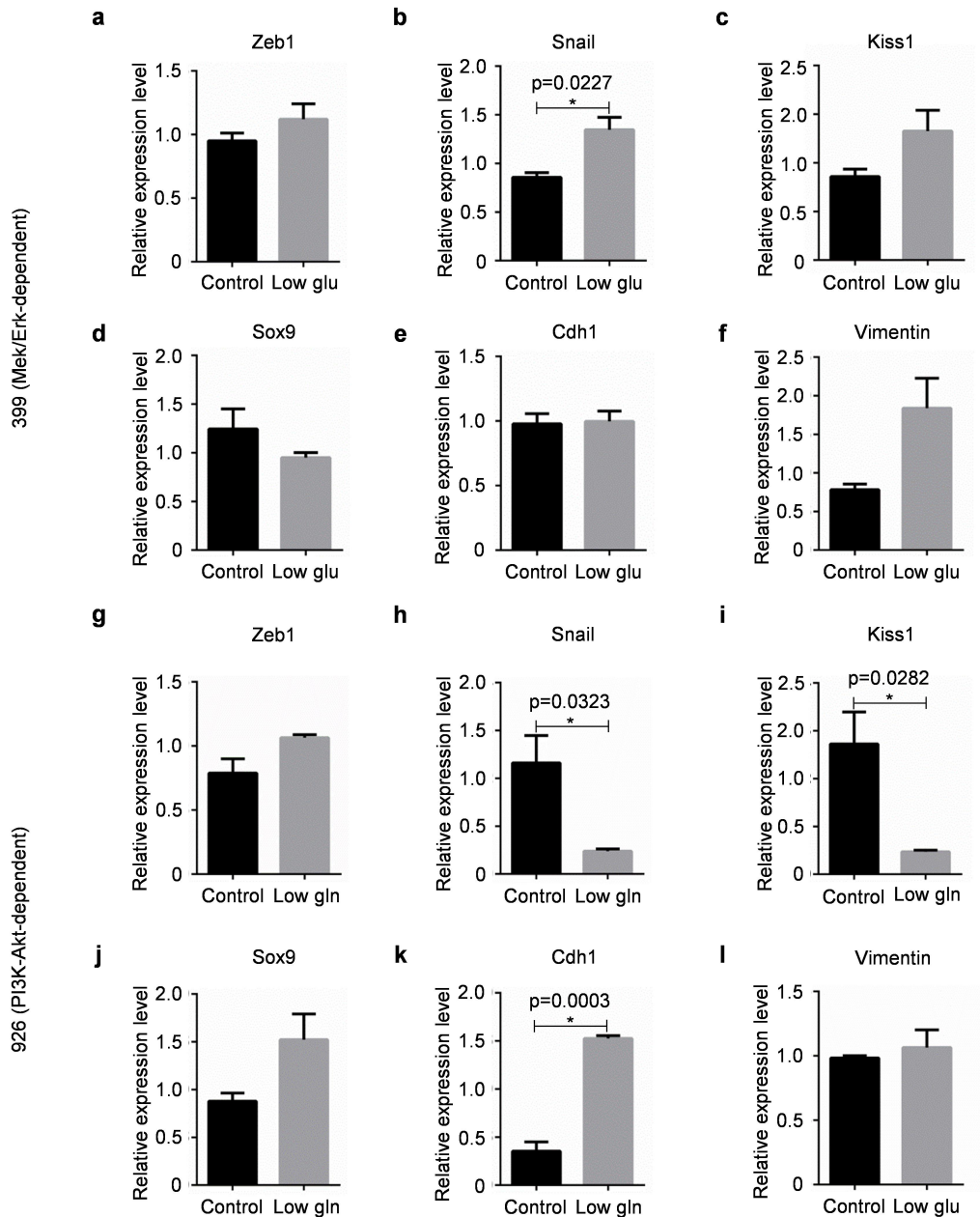
Figure 13. (a-f) QRT-PCR assays of Zeb1, Snail, Kiss1, Sox9, Cdh1, and Vimentin show that Mek/Erk-dependent cells exhibit more mesenchymal characteristics in the low-glucose group, **(g-l)** The mRNA levels of Zeb1, Snail, Kiss1, Sox9, Cdh1, and Vimentin show that PI3K/Akt-dependent cells display more epithelial characteristics in the low-glutamine group**.** All data are presented as means ± SEM of three independent experiments; statistical significance is determined by an unpaired *t*-test, where *p* < 0.05.

4.5.2.2 ER stress may not be involved

Nutrient deprivation is reported to induce ER stress [78]; meanwhile, tumour cells often undergo persistent ER stress [79]. There is evidence indicating that ER stress activation contributes to the invasion and migration ability of human cancer cells [56, 80]. Thus, we investigated the expression of a number of ER stress-related proteins including Bip, Chop, Pdi, and p-elf2α in adaptive cells and their counterparts (Figure 14). In 399 cells, no difference was observed. In 926 cells, the phosphorylation form of elf2α was found to be down-regulated in the low-glutamine group.
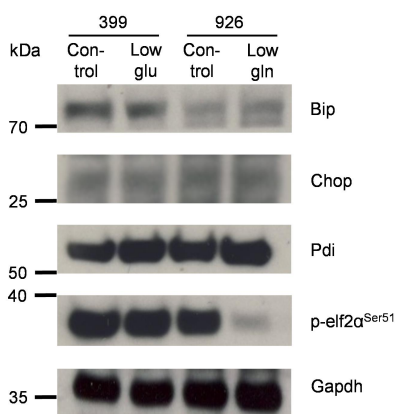
Figure 14. The western blot result shows the expression of Bip, Chop, Pdi and p-elf2α in adaptive cells and their parental cells.

4.5.2.3 PI3K/Akt-dependent cells show reduced activities in apoptosis, autophagy and mTOR

The nutrient-deprivation environment may not change one single pathway: harsh conditions triggers cell responses and the involved target genes or pathways interact as a collaborative network.

Indeed, our study shows that the invasive subgroup exhibited anti-apoptosis characteristics (with down-regulation of cleaved Caspase-3 protein expression), which existed in both Mek/Erk-dependent and PI3K/Akt-dependent cell lines (Figure 15).

Kim et al. reported that a nutrient-deprivation environment inhibited Akt activity and induced Ampk-mTOR pathway activation in the PANC-1 cell line, which prompted autophagy activation and anti-apoptosis [4]. Thus, we also examined the induction of Ampk-mTOR pathway and autophagy in our experimental setup. In 399 cells, no difference in phosphorylation levels of Ampkα, phospho-mTOR, and LC3B was observed. In 926 cells, phosphorylation levels of mTOR and LC3B were reduced while no difference was seen in Ampkα phosphorylation; this indicated that autophagy and mTOR might be diminished in the adaptive PI3K/Akt-dependent cells (Figure 15).
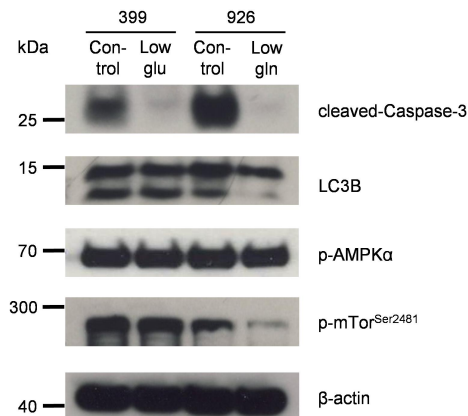
Figure 15. Western blot results show the expression of cleaved-Caspase-3 and LC3B as well as phosphorylation levels of AMPKα and mTOR in adaptive 399 and 926 cells.

4.6 Transcriptional profiling upon nutritional adaptation

To further understand biological changes after nutritional adaptation, we performed a microarray assay. Using 0.001 as the statistical cut-off for false discovery rate (FDR), 133 genes and 1,007 genes were differentially expressed in 399 and 926 cells respectively (the top 100 genes are listed in Supplementary Table 1.2). The KEGG (Kyoto Encyclopedia of Genes and Genomes) pathway analysis revealed that pathways related to regulation of peptidase activity, angiogenesis, and vasculature development appeared to be the most relevant ones responsible for adaptive changes of Mek/Erk-dependent cells to the glucose-limited environment (Table 2). Regarding PI3K/Akt-dependent cells, pathways associated with regulation of cellular component movement, locomotion, and cell migration seem to be involved (Table 3).

After nutritional adaptation, both 399 and 926 cells acquire invasive and anti-apoptotic properties. To verify if a metastatic phenotype also existed *in vivo*, we employed mouse model to examine the biological behaviour of the invasive subgroup *in vivo*. Considering that cell line, 926 could not form tumours in C57BL/6J (WT) mice, *in vivo* experiment was only performed on the 399 cell line.

Table 2. KEGG pathway analysis in Mek/Erk-dependent cell line 399

GOBPID	*p* value	Count	Size	Term
GO:0052547	1.05E-06	12	319	regulation of peptidase activity
GO:0010466	5.79E-06	9	199	negative regulation of peptidase activity
GO:0045765	7.83E-06	8	156	regulation of angiogenesis
GO:0001525	8.09E-06	11	324	angiogenesis

GO:0001944	1.47E-05	13	484	vasculature development
GO:1901342	1.53E-05	8	171	regulation of vasculature development
GO:0051346	2.16E-05	10	295	negative regulation of hydrolase activity
GO:0044767	6.75E-05	42	3,722	single-organism developmental process
GO:0032502	7.54E-05	42	3,739	developmental process
GO:0043086	9.28E-05	12	499	negative regulation of catalytic activity
GO:0051336	1.58E-04	15	785	regulation of hydrolase activity
GO:0048514	1.63E-04	9	305	blood vessel morphogenesis
GO:0052548	2.40E-04	8	254	regulation of endopeptidase activity
GO:0044092	2.73E-04	13	646	negative regulation of molecular function
GO:0050790	3.23E-04	20	1,335	regulation of catalytic activity
GO:0009653	3.46E-04	24	1,775	anatomical structure morphogenesis
GO:0045766	3.62E-04	5	94	positive regulation of angiogenesis
GO:0048646	4.83E-04	14	777	anatomical structure formation involved in morphogenesis
GO:0022603	4.90E-04	12	598	regulation of anatomical structure morphogenesis
GO:0009611	4.97E-04	12	599	response to wounding
GO:0050678	5.73E-04	7	220	regulation of epithelial cell proliferation

GO:0001568	5.75E-04	9	362	blood vessel development
GO:0072358	6.10E-04	12	613	cardiovascular system development
GO:0072359	6.10E-04	12	613	circulatory system development
GO:0071622	6.18E-04	3	26	regulation of granulocyte chemotaxis
GO:0043281	6.50E-04	6	162	regulation of cysteine-type endopeptidase activity involved in apoptotic process
GO:0048731	7.27E-04	31	2,702	system development
GO:0043491	7.43E-04	5	110	protein kinase B signaling
GO:0048856	7.81E-04	35	3,217	anatomical structure development
GO:2000116	9.16E-04	6	173	regulation of cysteine-type endopeptidase activity

Table 2. Top 30 pathways involved in PI3K/Akt-dependent cell line 926 from

KEGG analysis

GOBPID	P value	Count	Size	Term
GO:0051270	2.98E-15	69	493	regulation of cellular component movement
GO:0040011	4.21E-15	108	998	locomotion
GO:0016477	6.82E-15	91	776	cell migration

GO:0048870	7.32E-15	96	843	cell motility
GO:0040012	8.80E-15	67	480	regulation of locomotion
GO:0051239	1.20E-14	156	1,719	regulation of multicellular organismal process
GO:2000145	6.00E-14	62	440	regulation of cell motility
GO:0070887	1.56E-13	118	1,197	cellular response to chemical stimulus
GO:0009605	2.98E-13	114	1,150	response to external stimulus
GO:0032879	3.26E-13	134	1,448	regulation of localisation
GO:0030334	4.81E-13	59	425	regulation of cell migration
GO:0006928	5.44E-13	109	1,088	cellular component movement
GO:0048518	4.30E-12	235	3,168	positive regulation of biological process
GO:0048583	9.31E-12	173	2,139	regulation of response to stimulus
GO:0051179	1.04E-11	269	3,798	localisation
GO:0050793	2.25E-11	128	1,442	regulation of developmental process
GO:0010033	2.75E-11	125	1,400	response to organic substance
GO:0006935	3.59E-11	49	350	chemotaxis
GO:0042330	3.59E-11	49	350	taxis
GO:0001944	3.84E-11	60	484	vasculature development

GO:0048584	6.03E-11	102	1,069	positive regulation of response to stimulus
GO:0012501	7.92E-11	115	1,269	programmed cell death
GO:0008219	9.10E-11	119	1,333	cell death
GO:0006950	9.63E-11	158	1,953	response to stress
GO:0006915	9.81E-11	113	1,243	apoptotic process
GO:0072358	1.03E-10	69	613	cardiovascular system development
GO:0072359	1.03E-10	69	613	circulatory system development
GO:0016265	1.10E-10	119	1,337	death
GO:0022603	2.38E-10	67	598	regulation of anatomical structure morphogenesis
GO:0001525	3.01E-10	45	324	angiogenesis

4.7 Adaptive Mek/Erk-dependent cells form less necrotic tumours with increased angiogenesis *in vivo*

To determine if the low-glucose adapted cells preserved its invasive ability, apoptosis resistance, and neovascularization capacity not just *in vitro* but *in vivo*, we performed an orthotopic transplantation. Histological examination of transplanted tumours formed by low-glucose adaptive cells revealed that tumour cells tended to infiltrate into adjacent tissue with a blurry front and less pronounced stromal reactions (Figure 16a). No difference in proliferation was observed (Figure 16b). However, less tissue necrosis (as demarcated by

Caix-positive cells, Figure 16c) and less apoptotic cells (as labelled by cleaved-caspase3) were observed in tumours formed by low-glucose adaptive cells as compared to that of parental cells (Figure 16c).

These data suggested that the glucose levels in tumour microenvironment can potentially shape tumour histology. To verify if it holds true in human diseases, we carefully evaluated the histology and the incidence of tumour necrosis in 90 human PDAC sections (Figure 16d). Meanwhile, the history of diabetes was retrospectively retrieved from our electric database. Among non-diabetic PDAC sections, the incidence of tumour necrosis was 26.2% (16/61) which was significantly lower than 41.4% (12/29) in diabetic PDAC sections (p= 0.14, Figure 16e). These data demonstrated that non-diabetic PDAC patients probably tend to have non-necrotic tumours, which is in line with our data in the mouse.

|	Necrosis	Non-necrosis	Total
Non-diabetes	16	45	61
Diabetes	12	17	29
Total	28	62	90
p value		0.14	
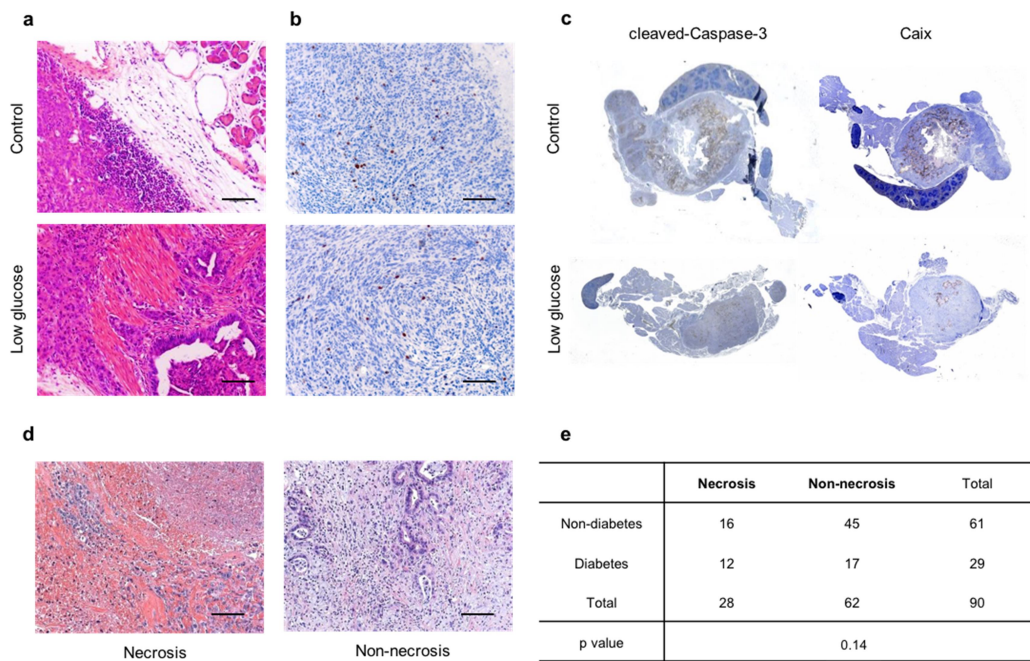
Figure 16. (a) Representative H&E staining images illustrate local invasive and less necrotic histological characteristics of transplanted tumour formed by

low-glucose adaptive cells; scale bar: 100 µm; **(b)** Representative IHC of p-PH-H3 pictures show no difference in proliferation; scale bar: 100 µm; **(c)** Representative images of IHC staining of cleaved-Caspase-3 (left) and Caix (right) groups show less apoptosis and necrosis area in tumours formed by low-glucose adaptive cells; n=4; **(d)** Representative H&E staining shows tumour histology of human necrotic and non-necrotic PDAC; scale bar: 100 µm; **(e)** Incidence of tumour necrosis in diabetic and non-diabetic PDAC sections; *p* value is calculated according to Chi-square test.

Since the *in vitro* microarray analysis prompted activation of angiogenesis pathways, the non-necrotic phenotype might be a consequence of angiogenesis activation. Thus we performed CD31 staining to assess microvessels in tumour tissue and quantified the vessel number and area. As expected, neovascularisation was more active in the low-glucose selected group with increased microvessel density (Figure 17a); meanwhile, there was an elevated Vegfa secretion in the low-glucose selected cells (Figure 17b). Since microarray data identified 13 genes differentially regulated in the angiogenesis process after low-glucose selection treatment (Figure 17c), we verified if the candidate genes were regulated similarly *in vivo*. As hypothesised, the Sparc gene, one of the most up-regulated genes was also significantly up-regulated in pancreatic orthotopically transplanted tumours (Figure 17c).

In summary, tumours formed by low-glucose adaptive cells displayed less necrotic tumours with increased local invasion, angiogenesis, and apoptosis resistance.
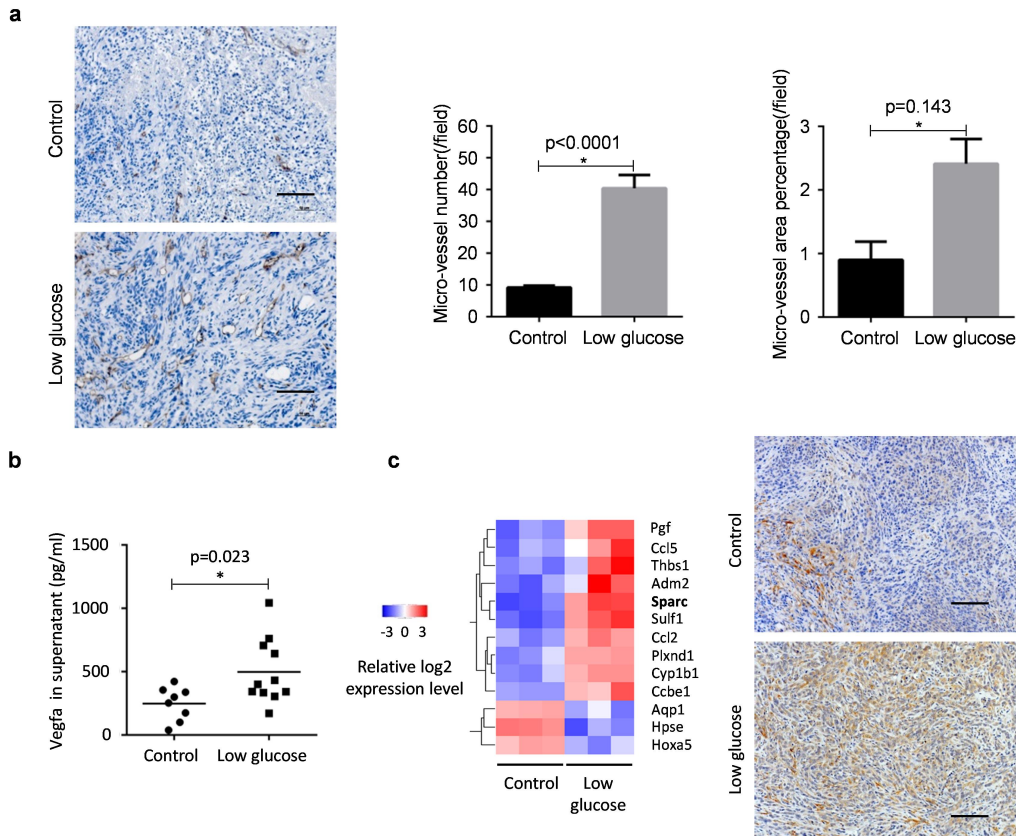
Figure 17. (a) IHC staining of CD31 shows active vascularization in transplanted tumours formed by low-glucose adaptive cells; scale bar: 100 µm; **(b)** Elisa results of mouse Vegfa shows higher Vegfa secretion in low-glucose adaptive cells; **(c)** A heat map of microarray analysis showing significantly regulated genes in angiogenesis after low-glucose adaptation; IHC staining of Sparc verifies microarray results; scale bar: 100 µm. The results are presented as a mean ± SEM; statistical significance was determined by an unpaired *t*-test, *: $p < 0.05$.

4.8 Low-glucose adaptation impairs remote tumour colonization

Above mentioned data suggested that the low-glucose adaptive cells were more invasive as compared to control cells; however, since no metastasis was observed in our orthotopic transplantation experiments, we used a portal vein injection to assess the metastatic potentials of these low-glucose adaptive

cells. Surprisingly, metastatic load in liver (as reflected by tumour areas in the liver) injected with low-glucose adaptive cells were remarkably lower than that of the control group (Figure 18a). The total metastasis area in the median lobe, left lobe, right lobe, and caudate lobe of the liver was five-fold lower in the low-glucose group than that in the control group (Figure 18b). Furthermore, these data were validated in tail vein injection model in which the low-glucose adaptive cells failed to form metastasis foci in lung (Figure 18c).
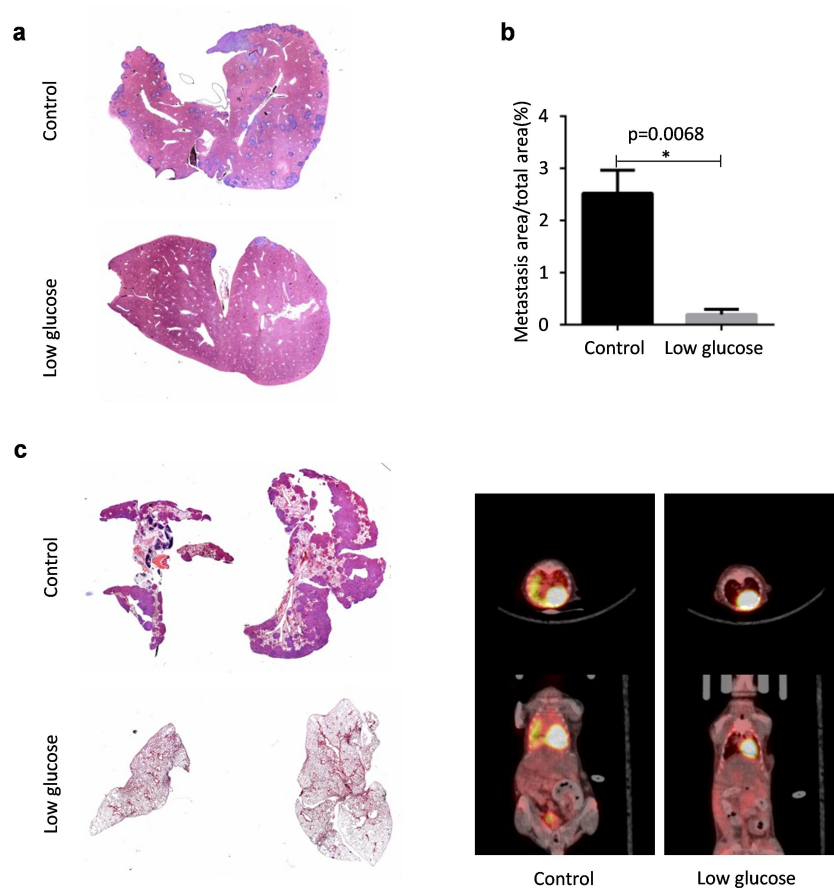
Figure 18. (a) H&E stained sections show significantly reduced metastasis in liver tissue after injection of 5×10^5 tumour cells through the portal vein; **(b)** The percentage of tumour area is significantly lower in low-glucose group (n=4) as compared to control group (n=4); **(c)** Representative H&E staining (left) and 18-F-PET scan images (right) show significantly reduced metastasis numbers in lung tissue after injection of 1×10^6 tumour cells through the tail vein (n=5).

The value is presented as a mean ± SEM; statistical significance is determined by an unpaired *t*-test, *: $p < 0.05$.

In order to form metastatic foci, tumour cells need to burst into blood vessels, endure under anchorage-independent conditions and adhere to new organs for survival and proliferation. Thus, it is likely that the low-glucose adaptive cells cannot survive in the blood stream before reaching remote organ. Thus, we first examined whether tumour cells survived in an anoikis state. No significant difference was observed (Figure 19a), suggesting the capacity to survive in the blood stream is not compromised. Since tumour colonization relies on their ECM proteins, we performed ECM array analysis under anoikis state. Interestingly, a number of ECM proteins related to colonization and adhesion were down-regulated (including Col3a1, Col6a1, Fbln1, Fn1, Itgax, Lama3, Spp1, Tgfbi, and Thbs1) in the low-glucose group as compared to control group (Figure 19b). Among them, Col6a1, Spp1, and Fn1, confirmed by QRT-PCR (Figure 19c), were previously shown to be associated with tumour colonization [81].
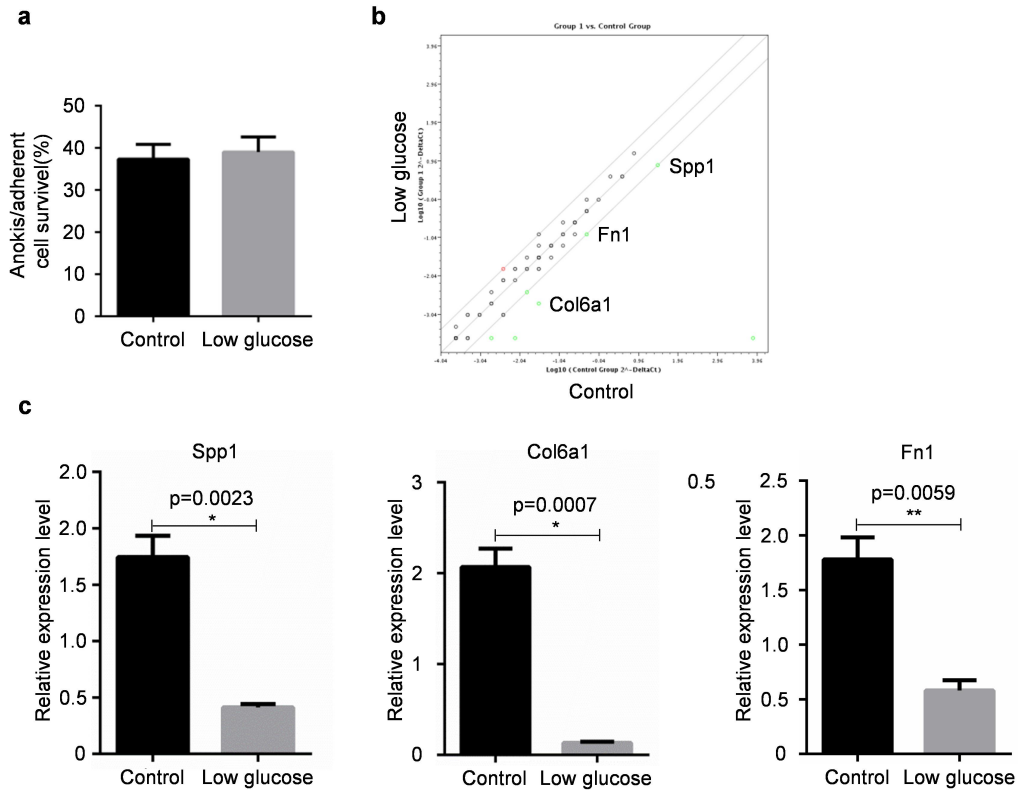
Figure 19. (a) Anoikis assay shows no difference in cell viability between the control cell and the low-glucose adaptive cells under an anoikis state; **(b)** ECM array shows differential expression in ECM proteins between low-group and control group; **(c)** QRT-PCR results verify mRNA expression level differences of Spp1 (left), Col6a1 (middle), and Fn1 (right) in both groups. All data are present as a mean ± SEM; statistical significance is determined by an unpaired *t*-test, *: *p* < 0.05.

5. DISCUSSION

In PDAC, oncogenic KRAS and its downstream signalling pathways such as MEK/ERK and PI3K/AKT signalling pathways are involved in malignant transformation [12]. Albeit the existence of clonal heterogeneity, it has been proposed that the dominant oncogenic signal may determine the phenotype of cancer cells [59].

One significant feature of PDAC is dense stroma which hinders the delivery of necessary nutrient [82, 83]. Furthermore, the poor vascularisation and fluctuation in the blood supply may pose additional obstacles [84]. PDAC cells sustain themselves with metabolism reprogramming under a temporary energy stress. However, this may restrict cell growth and affect biological behaviour [85]. Recently, Yun's research group found that colorectal cancer cells maintained in a low-glucose environment for 30 days acquired KRAS and BRAF gene mutation [86]. These data revealed a link among nutrient dependency, environmental status and acquisition of oncogenic mutations. The data also suggested that an abnormal microenvironment may constitute an extrinsic trigger for genomic instability.

Since the 1980s, scientists have been dedicated to recapitulate pancreatic cancer phenotypes in genetically engineered mouse models (GEMMs). Over time, GEMMs have been verified to replicate primary pathological progress of human PDAC and have been successfully applied in the research field [87]. Previously, we have established a set of GEMMs. Here, we characterised a PDAC subtype which is driven by Kras/Mek/Erk cascade while another cystic subtype is initiated by PI3K/Akt cascade [59]. The KEGG pathway analysis revealed that glycolysis/gluconeogenesis played a vital role in mediating

Kras/Erk-driven pancreatic carcinogenesis [59]. These data underlie the im-importance of crosstalk between the dominant oncogenic pathway and tumour metabolism in mediating pancreatic transformation.

Here, we hypothesised that the dominant oncogenic pathway might influence the metabolic phenotype of PDAC. To test this, we exposed the murine PDAC cells (Mek/Erk-dependent vs. PI3K/Akt-dependent) to the nutrient-limited culture medium (glucose-depleted vs. glutamine-depleted). Since glutamine is a major source of carbon and nitrogen, the tested cells did not survive under the glutamine-depleted culture medium.

Cells with activation of PI3K/Akt signalling (PI3K/Akt-dependent and duo-dependent) could better adapt to glucose-free conditions. The formed colony numbers only reduced around 10% for PI3K/Akt-dependent cells, and 50% for duo-dependent cells (Figure 4). In this respect, this result suggested that Mek/Erk-dependent cells were less resistant to the deprivation of glucose in comparison to that of PI3K/Akt-dependent cells.

However, when a minimal amount of nutrient is provided, the impaired growth rate of Mek/Erk-dependent and PI3K/Akt-dependent cells was restored immediately. In line, previous studies in the malignant haematological tumour have shown that cancer cells are capable of rescuing growth rates and macromolecule synthesis by adjusting to other types of nutrient acquisition under the conditions of nutrient deprivation [88].

Although the nutrient limit response is quick, efficient, it involves activation of some major pathways, such as AMPK, AKT, ERK, or mTOR [89], when

encountering extended periods of nutritional deprivation, cancer cells must launch cascades of events to resolve a stressful metabolic situation.

Early attempts to discuss the relationship among metabolic environment, oncogene addiction, and potential involving mechanisms focused on acute, short-term situations. The experimental cells were maintained in a nutrient-deprived environment for as long as 120 hours [90-92]. However, tumour growth *in vivo* was a relatively long period and accompanied with the nutrient shortage and renewal. To faithfully recapitulate this, we designed our experiments to mimic the nutrient fluctuation *in vivo* and to investigate its influence on cellular behaviours (Figure 6).

To survive in the nutrient-limited environment, tumour cells needed to increase the nutrient intake or switch off the energy-consuming pathway to store energy and macromolecules for proliferation. Our results showed that Mek/Erk-dependent cells improve the energy supply by increasing glucose uptake (Figure 9a). While PI3K/Akt-dependent cells by inhibiting Akt and mTOR phosphorylation (Figure 7, Figure 15), indicating energy preservation by down-regulating the most energy-consumption mTOR signalling pathway [93]. Both strategies appeared to be sufficient to maintain intracellular energy status because ATP and ADP production were elevated in adapted cells (Figure 11). However, the anti-ROS accumulation response existed only in PI3K/Akt-dependent cells (Figure 10). One possible explanation for this might be a feedback loop between PI3K/AKT signalling and ROS. Indeed, on the one hand, Akt activation contributed to intracellular ROS accumulation by way of intervention from the forkhead box O (FOXO) family and from stimulating mitochondria oxidative metabolism [94]. On the other hand, ROS accumulation

led to inactivation of Pten, which ultimately caused Akt activation [95]. Taken together, how cancer cells adapt to the nutrient-limited condition is affected by the operating dominant oncogenic pathway.

In Mek/Erk-dependent cells, the low-glucose culture medium selects the invasive clones while the low-glutamine medium selects invasive clones in PI3K/Akt-dependent cells.

Given the high energy circulating state in the invasive cells, a possible explanation was that adaptive cells produced and consumed more energy to initiated invasion related pathways to evade from the limited nutrient environment.

To test this hypothesis, we investigated pathways related to cellular invasions such as EMT, apoptosis, autophagy and ER stress [44, 96, 97]. In PDAC, EMT is a classical pathogenesis related to the malignant transformation of tumour cells [98]. Thus, we tested whether EMT is associated with the invasive phenotype induced by the environmental adaption. Interestingly, EMT is not altered in these adaptive cells.

Another important feature of adaptive change is the acquisition of apoptosis resistance. It is still under debate whether a nutrient-deprived environment promotes or inhibits apoptosis. Cultured in the low-glucose medium for seven days, apoptosis was induced in rat pancreatic β-cells [99]. Glucose deprivation was found to induce Caspase-8-mediated apoptosis in Bax-, Bak-deficient cells [100]. These data argue for a supportive role of low glucose in inducing apoptosis. However, other studies demonstrated that glucose or serum exerts

apoptosis-inhibitory effects and promotes cell survival under nutrient depriva-deprivation [101, 102]. In our current study, PDAC cells were maintained the nutrient-limitation condition for long periods and the subsequence adaptive changes have taken place, thus, it is likely that apoptosis was suppressed instead of activated in the process of low-glucose adaptation.

To conclude, when the preferred nutrient was limited in the microenvironment, the common response of PDAC cells is to initiate invasion and to acquire apoptosis resistance.

To assess the overall impact of nutrient deprivation on genes expression, we performed a microarray analysis. Here, a number of genes were differently expressed (133 for Mek/Erk-dependent cells and 1007 for PI3K/Akt cells). Moreover, 30 pathways were regulated after glucose-deprivation selection in Mek/Erk-dependent cells while 314 in PI3K/Akt-dependent cells accordingly. By analysing these pathways, we observe that PI3K/Akt-dependent cells were more flexible in responding to low-energy stress by regulating various mechanisms such as apoptosis, autophagy, Akt/mTOR signalling and phosphorylation of transduction factor elf-2α, leading to a better adaptation to the harsh environment (Figure 15).

The major pathways involved in response to the energy crisis in Mek/Erk-dependent cells were angiogenesis regulation and vasculature development. Angiogenesis has long been considered as one of the hallmarks of cancer [25].

Despite various discussion on the biological significance of angiogenesis, it is generally accepted that 1) blood vessel remodelling exists extensively in cancer despite the fact that some tumour-associated vessels are rough and unfunctional; 2) tumour microenvironment governs angiogenesis, and, in return, angiogenesis influences the components and structure of tumour microenvironments; 3) the interplay inside angiogenesis among various factors are extremely active [103]. The Mek/Erk-dependent cell lines were isolated from murine PDAC tissues with pronounced necrosis [104]; thus, the low blood perfusion renders them more vulnerable to the low-glucose environment. Previously, it has been reported that, under a low-glucose condition, Vegfa production was up-regulated in rat kidney cells, human vascular smooth muscle cells and human lymphoma cell lines [105, 106]. The microarray data showed that switching to angiogenesis in Mek/Erk-dependent cells was the consequence of series of molecular events including elevated Vegfa secretion, destruction of ECM (Sparc) and crosstalk with receptors (Plexd1) (Figure 17). Taken together, Mek/Erk-dependent cells adapted to a low-glucose environment by switching to angiogenesis while PI3K/Akt-dependent cells mainly adapted by co-regulating of various signalling pathways.

Since the PI3K/Akt-dependent cell do not form a tumour in WT mice, we performed only *in vivo* experiment using Mek/Erk-dependent cells.

An interesting finding in our study is that the low-glucose selected Mek/Erk-dependent cells reversed their well-characterized necrotic phenotype [59, 104]; moreover, a similar conclusion could be drawn from PDAC patients

without diabetes (Figure 16). It has been recognised that diabetes is related to carcinogenesis and the progression of pancreatic cancer, while the underlying mechanism remains unknown [107]. Under normal culture conditions, PDAC cells were cultured in a high glucose medium (25 mM) *in vitro*, the actual blood glucose concentration in a healthy human is 5.5 mM [108]. Here, Mek/Erk-dependent cells cultured in low-glucose concentrations to some degree represents PDAC patients without diabetes. The adaptive cells (to low glucose culture condition) switched on the angiogenic process with reduced tumour necrosis. Since tumour necrosis is correlated with poor prognosis [109, 110], our data provided an explanation for the unfavourable outcomes for PDAC patients with diabetes.

Another pivotal finding in our study is that the low-glucose selected cells show increased local invasion while they form significantly less number of metastatic foci in distant target organs, suggesting a compromised ability of tumour colonization (Figure 18). A possible explanation may be the lack of adhesion and colonization ability. Costa-Silva and his team reported that, even before migrating to distant organs, pancreatic cancer cells derived exosomes to "pre-educate" the target organ - for example, the liver to build an environment that favoured their metastasis. This pre-education included mainly on up-regulation of ECM protein [111]. Paron described in a publication that a Tnc-rich matrix is required for migration and adhesion of human pancreatic cancer cell line Su86.86 and Panc-1 *in vitro* [112]. These findings proved that a relatively "sticky" microenvironment was extremely beneficial for adhesion and colonization in the target organ. Loss of key ECM proteins influenced tumour

colonization. In our study, the ECM array result found that, after exposed to anoikis conditions for 24 hours, the low-glucose-selected cells reduced the expression of a number of key ECM proteins such as Col6a1, Spp1, and Fn1. It can, therefore, be assumed that, after low-glucose selection treatment, the Kras mutant murine PDAC cells acquire angiogenesis ability and apoptosis resistance; however, they were not able to build an adhesive matrix for the colonization in the new target organ. The detailed underlying mechanism remains to be explained by further work.

6. SUMMARY

In this study, we demonstrated that major energy source (glucose-dependent vs. glutamine-dependent) was affected by dominant oncogenic signal (Mek/Erk-dependent vs. PI3K/Akt-dependent). The nutritionally stressful condition (e.g. lack of essential source for energy production) tends to select the PDAC cells with locally aggressive and angiogenic phenotype; however, they were deficient in remote colonization. Furthermore, this nutritional adaption affects the tumour histology in that the Mek/Erk-dependent cancer cells adaptive to the low-glucose level were less likely to give rise to a necrotic tumour *in vivo* (see below).

The questions proposed in the 'AIM OF THIS STUDY' section have been answered as follows:

Question 1 (Q1): What is the association between the dominant cancer signal and the nutritional requirement for cell proliferation?

Conclusion 1 (C1): By comparing two groups of PDAC cell lines with disparate dominant cancer signals (Mek/Erk-dependent vs. PI3K/Akt-dependent), we observed that Mek/Erk-dependent cells rely on glucose for proliferation; however, the PI3K/Akt-dependent cells rely on glutamine instead.

Question 2 (Q2): Which cell lines are able to maintain the proliferative potential under the nutritionally stressful condition?

Conclusion 2 (C2): Both the Mek/Erk-dependent and the PI3K/Akt-dependent cell lines were able to maintain the proliferative potential under the minimal culture condition, given that the preferred energy source was present (e.g.

glucose for Mek/Erk-dependent cells, and glutamine for PI3K/Akt-dependent cells).

Question 3 (Q3): How do cancer cells respond to the nutritionally stressful condition *in vitro*, for instance, when the preferred energy source is provided only in a limited concentration?

Conclusion 3 (C3): A similar phenotype was observed in the Mek/Erk-dependent and the PI3K/PI3K/Akt-dependent cells once they were adapted to the nutritionally stressful condition *in vitro*: both of them maintained a similar proliferation rate, and they acquired apoptosis resistance and a locally aggressive/invasive phenotype.

Question 4 (Q4): How does the nutritional adaption alter the tumour histological and biological phenotype *in vivo*?

Conclusion 4 (C4): The Mek/Erk-dependent cancer cells adaptive to the low-glucose levels were more angiogenic, locally aggressive, and less likely to form necrotic tumour histology as their parenteral clones. However, they simultaneously lose the capacity to colonize distant organs, such as the liver and the lungs.

7. ABBREVIATIONS

ADP	Adenosine diphosphate
AKT	Protein kinase B
AMPK	AMP-activated protein kinase
ATF6α	Activating transcription factor 6α
ATP	Adenosine triphosphate
BCL-2	B-cell lymphoma 2
BiP	Heat shock 70kDa protein 5
BSA	Bovine serum albumin
Caix	Carbonic anhydrase 9
Casp3	Caspase 3
CD31	platelet/endothelial cell adhesion molecule 1
CDH1	Cadherin
CDKN2A	Cyclin-dependent kinase Inhibitor 2A
CHOP	C/EBP homologous protein
COL3A1	Collagen, Type III, Alpha 1
COL6A1	Collagen, Type VI, Alpha 1
Cre	Cre recombinase
DG6P	2-Deoxy-Glucose-6-Phosphate
ECM	Extracellular matrix
eIF2α	Eukaryotic translation initiation factor 2α

EGFR	Epidermal growth factor receptor
EMT	Epithelial-to-mesenchymal transition
ER	Endoplasmic reticulum
ERK	Extracellular signal-regulated kinase
FBLN1	Fibulin 1
FBS	Fetal bovine serum
FDR	False discovery rate
FGF	Fibroblast growth factor
FN1	Fibronectin 1
GAPDH	Glyceraldehyde-3-phosphate dehydrogenase
GCN2	Eukaryotic translation initiation factor 2 alpha kinase 4
GDP	Guanosine diphosphate
GEMM	Genetically engineered mouse model
GPX	Glutathione peroxides
GRB10	Growth factor receptor-bound protein 10
GRP78	78-kDa glucose regulated protein
GTP	Guanosine triphosphate
HRI	Eukaryotic translation initiation factor 2-alpha kinase
HRP	Horseradish peroxidase
IGF-1	Insulin-like growth factor-1
IHC	Immunohistochemistry
IRE1α	Inositol requiring enzyme 1 alpha

ITGAX	Integrin, alpha X
ITGB3	Integrin, beta 3
KCl	Potassium chloride
KEGG	Kyoto Encyclopedia of Genes and Genomes
KISS1	KiSS-1 metastasis suppressor
KRAS	V-Ki-ras2 Kirsten rat sarcoma viral oncogene homolog
LAMA3	Laminin alpha 3
LAMB3	Laminin beta 3
LKB1	Serine/threonine kinase 11
MAPK	Mitogen-activated protein kinase
MLH1	MutL Homolog 1
MSH2	MutS Homolog 2
mTOR	Mammalian target of rapamycin
mTORC1	mTOR complex1
mTORC2	mTOR complex 2
MTT	3-(4,5-dimethylthiazole-2-yl)2,5-diphenyltetrazolium bromide
$NADP^+$	Nicotinamide adenine dinucleotide phosphate
NADPH	Reduction form of $NADP^+$
NF-κB	Nuclear factor of kappa light polypeptide gene enhancer in B cells 1
p16	Cyclin-dependent kinase inhibitor 2A
p48	Pancreas specific transcription factor, 1a
p53	Tumour protein p53

PALB2	Partner and localizer of BRCA2
PARP1	Poly (ADP-ribose) polymerase 1
PBS	Phosphate buffered saline
PCD	Programmed cell death
PDAC	Pancreatic ductal adenocarcinoma
PDGF	Platelet-derived growth factor
PDI	Pancreas-specific protein disulfide isomerase
PERK	PRKR-like endoplasmic reticulum kinase
PI3K	Phosphatidylinositol-4,5-bisphosphate 3-kinase
PIP3	Phosphatidylinositol (3,4,5)-trisphosphate
PIP2	Phosphatidylinositol 4,5-bisphosphate
PKR	Eukaryotic translation initiation factor 2 alpha kinase 2
PTEN	Phosphatase and tensin homolog
REDD1	DNA-damage-inducible transcript 4
RIP	Receptor interacting protein
Rma	Robust multichip average
ROS	Reactive oxygen species
SDS	Laurylsulfate
SLUG	Snail family zinc finger 2
SMAD4	SMAD family member 4
SNAIL	Snail family zinc finger 1
SOD	Superoxide dismutase

SOX9	SRY (Sex Determining Region Y)-box 9
SPARC	Secreted protein acidic and rich in cysteine
SPP1	Secreted phosphoprotein 1
TCA	Tricarboxylic acid cycle
TGFBI	Transforming growth factor beta-induced
THBS1	Thrombospondin 1
TNF	Tumour necrosis factor
TSC	Tuberous sclerosis
UPR	Unfold-fold protein response
VEGF	Vascular endothelial growth factor
WB	Western blot
ZEB1	Zinc finger e-box binding homeobox 1
ZEB2	Zinc finger e-box binding homeobox 2
α-SMA	α-smooth muscle actin

8. REFERENCES

[1] Rahib L., Smith B. D., Aizenberg R., Rosenzweig A. B., Fleshman J. M. & Matrisian L. M. (2014). Projecting cancer incidence and deaths to 2030: the unexpected burden of thyroid, liver, and pancreas cancers in the United States. *Cancer Res*, 74(11), 2913-2921.

[2] Siegel R. L., Miller K. D. & Jemal A. (2015). Cancer statistics, 2015. *CA Cancer J Clin*, 65(1), 5-29.

[3] Hall P. A. & Lemoine N. R. (1993). Models of pancreatic cancer. *Cancer Surv*, 16, 135-155.

[4] Kim S. E., Park H. J., Jeong H. K., Kim M. J., Kim M., Bae O. N. & Baek S. H. (2015). Autophagy sustains the survival of human pancreatic cancer PANC-1 cells under extreme nutrient deprivation conditions. *Biochem Biophys Res Commun*, 463(3), 205-210.

[5] Mihaljevic A. L., Michalski C. W., Friess H. & Kleeff J. (2010). Molecular mechanism of pancreatic cancer--understanding proliferation, invasion, and metastasis. *Langenbecks Arch Surg*, 395(4), 295-308.

[6] Hruban R. H. & Adsay N. V. (2009). Molecular classification of neoplasms of the pancreas. *Hum Pathol*, 40(5), 612-623.

[7] Agarwal A. & Saif M. W. (2014). KRAS in pancreatic cancer. *JOP*, 15(4), 303-305.

[8] Hingorani S. R., Petricoin E. F., Maitra A., Rajapakse V., King C., Jacobetz M. A., Ross S., Conrads T. P., Veenstra T. D., Hitt B. A., Kawaguchi Y., Johann D., Liotta L. A., Crawford H. C., Putt M. E., Jacks T., Wright C. V., Hruban R. H., Lowy A. M. & Tuveson D. A. (2003). Preinvasive and invasive ductal pancreatic cancer and its early detection in the mouse. *Cancer Cell*, 4(6), 437-450.

[9] Ying H., Kimmelman A. C., Lyssiotis C. A., Hua S., Chu G. C., Fletcher-Sananikone E., Locasale J. W., Son J., Zhang H., Coloff J. L., Yan H., Wang W., Chen S., Viale A., Zheng H., Paik J. H., Lim C., Guimaraes A. R., Martin E. S., Chang J., Hezel A. F., Perry S. R., Hu J., Gan B., Xiao Y., Asara J. M., Weissleder R., Wang Y. A., Chin L., Cantley L. C. & DePinho R. A. (2012). Oncogenic Kras maintains pancreatic

tumors through regulation of anabolic glucose metabolism. *Cell*, 149(3), 656-670.

[10] Roberts P. J. & Der C. J. (2007). Targeting the Raf-MEK-ERK mitogen-activated protein kinase cascade for the treatment of cancer. *Oncogene*, 26(22), 3291-3310.

[11] Neuzillet C., Hammel P., Tijeras-Raballand A., Couvelard A. & Raymond E. (2013). Targeting the Ras-ERK pathway in pancreatic adenocarcinoma. *Cancer Metastasis Rev*, 32(1-2), 147-162.

[12] Schonleben F., Qiu W., Ciau N. T., Ho D. J., Li X., Allendorf J. D., Remotti H. E. & Su G. H. (2006). PIK3CA mutations in intraductal papillary mucinous neoplasm/carcinoma of the pancreas. *Clin Cancer Res*, 12(12), 3851-3855.

[13] Sarkar F. H., Banerjee S. & Li Y. (2007). Pancreatic cancer: pathogenesis, prevention and treatment. *Toxicol Appl Pharmacol*, 224(3), 326-336.

[14] Huang K. & Fingar D. C. (2014). Growing knowledge of the mTOR signaling network. *Semin Cell Dev Biol*, 36, 79-90.

[15] Dibble C. C. & Cantley L. C. (2015). Regulation of mTORC1 by PI3K signaling. *Trends Cell Biol*, 25(9), 545-555.

[16] Gaubitz C., Prouteau M., Kusmider B. & Loewith R. (2016). TORC2 Structure and Function. *Trends Biochem Sci*, 41(6), 532-545.

[17] Kennedy A. L., Morton J. P., Manoharan I., Nelson D. M., Jamieson N. B., Pawlikowski J. S., McBryan T., Doyle B., McKay C., Oien K. A., Enders G. H., Zhang R., Sansom O. J. & Adams P. D. (2011). Activation of the PIK3CA/AKT pathway suppresses senescence induced by an activated RAS oncogene to promote tumorigenesis. *Mol Cell*, 42(1), 36-49.

[18] Mendoza M. C., Er E. E. & Blenis J. (2011). The Ras-ERK and PI3K-mTOR pathways: cross-talk and compensation. *Trends Biochem Sci*, 36(6), 320-328.

[19] Steelman L. S., Chappell W. H., Abrams S. L., Kempf R. C., Long J., Laidler P., Mijatovic S., Maksimovic-Ivanic D., Stivala F., Mazzarino M. C., Donia M., Fagone P., Malaponte G., Nicoletti F., Libra M., Milella M., Tafuri A., Bonati A., Basecke J., Cocco L., Evangelisti C., Martelli A. M., Montalto G., Cervello M. & McCubrey J. A. (2011). Roles of the Raf/MEK/ERK and

PI3K/PTEN/Akt/mTOR pathways in controlling growth and sensitivity to therapy-implications for cancer and aging. *Aging (Albany NY)*, 3(3), 192-222.

[20] Weinstein I. B. (2000). Disorders in cell circuitry during multistage carcinogenesis: the role of homeostasis. *Carcinogenesis*, 21(5), 857-864.

[21] Dang C. V. (2012). Links between metabolism and cancer. *Genes Dev*, 26(9), 877-890.

[22] Spill F., Reynolds D. S., Kamm R. D. & Zaman M. H. (2016). Impact of the physical microenvironment on tumor progression and metastasis. *Curr Opin Biotechnol*, 40, 41-48.

[23] Yanagisawa K., Konishi H., Arima C., Tomida S., Takeuchi T., Shimada Y., Yatabe Y., Mitsudomi T., Osada H. & Takahashi T. (2010). Novel metastasis-related gene CIM functions in the regulation of multiple cellular stress-response pathways. *Cancer Res*, 70(23), 9949-9958.

[24] Kimbro K. S. & Simons J. W. (2006). Hypoxia-inducible factor-1 in human breast and prostate cancer. *Endocr Relat Cancer*, 13(3), 739-749.

[25] Hanahan D. & Weinberg R. A. (2011). Hallmarks of cancer: the next generation. *Cell*, 144(5), 646-674.

[26] Kamphorst J. J., Nofal M., Commisso C., Hackett S. R., Lu W., Grabocka E., Vander Heiden M. G., Miller G., Drebin J. A., Bar-Sagi D., Thompson C. B. & Rabinowitz J. D. (2015). Human pancreatic cancer tumors are nutrient poor and tumor cells actively scavenge extracellular protein. *Cancer Res*, 75(3), 544-553.

[27] Blum R. & Kloog Y. (2014). Metabolism addiction in pancreatic cancer. *Cell Death Dis*, 5, e1065.

[28] Daemen A., Peterson D., Sahu N., McCord R., Du X., Liu B., Kowanetz K., Hong R., Moffat J., Gao M., Boudreau A., Mroue R., Corson L., O'Brien T., Qing J., Sampath D., Merchant M., Yauch R., Manning G., Settleman J., Hatzivassiliou G. & Evangelista M. (2015). Metabolite profiling stratifies pancreatic ductal adenocarcinomas into subtypes with distinct sensitivities to metabolic inhibitors. *Proc Natl Acad Sci U S A*, 112(32), E4410-7.

[29] Yu M., Zhou Q., Zhou Y., Fu Z., Tan L., Ye X., Zeng B., Gao W., Zhou J., Liu Y., Li Z., Lin Y., Lin Q. & Chen R. (2015). Metabolic phenotypes in pancreatic cancer. *PLoS One*, 10(2), e0115153.

[30] Dang C. V. (2010). Glutaminolysis: supplying carbon or nitrogen or both for cancer cells? *Cell Cycle*, 9(19), 3884-3886.

[31] Menendez J. A., Oliveras-Ferraros C., Cufi S., Corominas-Faja B., Joven J., Martin-Castillo B. & Vazquez-Martin A. (2012). Metformin is synthetically lethal with glucose withdrawal in cancer cells. *Cell Cycle*, 11(15), 2782-2792.

[32] Laubenbacher R., Hower V., Jarrah A., Torti S. V., Shulaev V., Mendes P., Torti F. M. & Akman S. (2009). A systems biology view of cancer. *Biochim Biophys Acta*, 1796(2), 129-139.

[33] Kerr J. F., Wyllie A. H. & Currie A. R. (1972). Apoptosis: a basic biological phenomenon with wide-ranging implications in tissue kinetics. *Br J Cancer*, 26(4), 239-257.

[34] Sankari S. L., Masthan K. M., Babu N. A., Bhattacharjee T. & Elumalai M. (2012). Apoptosis in cancer--an update. *Asian Pac J Cancer Prev*, 13(10), 4873-4878.

[35] Wong R. S. (2011). Apoptosis in cancer: from pathogenesis to treatment. *J Exp Clin Cancer Res*, 30, 87.

[36] Szegezdi E., Fitzgerald U. & Samali A. (2003). Caspase-12 and ER-stress-mediated apoptosis: the story so far. *Ann N Y Acad Sci*, 1010, 186-194.

[37] Hamacher R., Schmid R. M., Saur D. & Schneider G. (2008). Apoptotic pathways in pancreatic ductal adenocarcinoma. *Mol Cancer*, 7, 64.

[38] Mizushima N., Yoshimori T. & Levine B. (2010). Methods in mammalian autophagy research. *Cell*, 140(3), 313-326.

[39] De Duve C. (1963). The lysosome. *Sci Am*, 208, 64-72.

[40] Sui X., Chen R., Wang Z., Huang Z., Kong N., Zhang M., Han W., Lou F., Yang J., Zhang Q., Wang X., He C. & Pan H. (2013). Autophagy and chemotherapy resistance: a promising therapeutic target for cancer treatment. *Cell Death Dis*, 4, e838.

[41] Ojha R., Bhattacharyya S. & Singh S. K. (2015). Autophagy in Cancer Stem Cells: A Potential Link Between Chemoresistance, Recurrence, and Metastasis. *Biores Open Access*, 4(1), 97-108.

[42] Dalby K. N., Tekedereli I., Lopez-Berestein G. & Ozpolat B. (2010). Targeting the prodeath and prosurvival functions of autophagy as novel therapeutic strategies in cancer. *Autophagy*, 6(3), 322-329.

[43] Perera R. M., Stoykova S., Nicolay B. N., Ross K. N., Fitamant J., Boukhali M., Lengrand J., Deshpande V., Selig M. K., Ferrone C. R., Settleman J., Stephanopoulos G., Dyson N. J., Zoncu R., Ramaswamy S., Haas W. & Bardeesy N. (2015). Transcriptional control of autophagy-lysosome function drives pancreatic cancer metabolism. *Nature*, 524(7565), 361-365.

[44] Dufey E., Urra H. & Hetz C. (2015). ER proteostasis addiction in cancer biology: Novel concepts. *Semin Cancer Biol*, 33, 40-47.

[45] Wang M., Wey S., Zhang Y., Ye R. & Lee A. S. (2009). Role of the unfolded protein response regulator GRP78/BiP in development, cancer, and neurological disorders. *Antioxid Redox Signal*, 11(9), 2307-2316.

[46] Wu J. & Kaufman R. J. (2006). From acute ER stress to physiological roles of the Unfolded Protein Response. *Cell Death Differ*, 13(3), 374-384.

[47] Rivas A., Vidal R. L. & Hetz C. (2015). Targeting the unfolded protein response for disease intervention. *Expert Opin Ther Targets*, 19(9), 1203-1218.

[48] Malhotra J. D. & Kaufman R. J. (2011). ER stress and its functional link to mitochondria: role in cell survival and death. *Cold Spring Harb Perspect Biol*, 3(9), a004424.

[49] Keleg S., Buchler P., Ludwig R., Buchler M. W. & Friess H. (2003). Invasion and metastasis in pancreatic cancer. *Mol Cancer*, 2, 14.

[50] Marcucci F., Bellone M., Caserta C. A. & Corti A. (2014). Pushing tumor cells towards a malignant phenotype: stimuli from the microenvironment, intercellular communications and alternative roads. *Int J Cancer*, 135(6), 1265-1276.

[51] Amaravadi R. K. & Thompson C. B. (2007). The roles of therapy-induced autophagy and necrosis in cancer treatment. *Clin Cancer Res*, 13(24), 7271-7279.

[52] Douma S., Van Laar T., Zevenhoven J., Meuwissen R., Van Garderen E. & Peeper D. S. (2004). Suppression of anoikis and induction of metastasis by the neurotrophic receptor TrkB. *Nature*, 430(7003), 1034-1039.

[53] Yang S., Wang X., Contino G., Liesa M., Sahin E., Ying H., Bause A., Li Y., Stommel J. M., Dell'antonio G., Mautner J., Tonon G., Haigis M., Shirihai O. S., Doglioni C., Bardeesy N. & Kimmelman A. C. (2011). Pancreatic cancers require autophagy for tumor growth. *Genes Dev*, 25(7), 717-729.

[54] Jiang S. H., Wang Y., Yang J. Y., Li J., Feng M. X., Wang Y. H., Yang X. M., He P., Tian G. A., Zhang X. X., Li Q., Cao X. Y., Huo Y. M., Yang M. W., Fu X. L., Li J., Liu D. J., Dai M., Wen S. Y., Gu J. R., Hong J., Hua R., Zhang Z. G. & Sun Y. W. (2016). Overexpressed EDIL3 predicts poor prognosis and promotes anchorage-independent tumor growth in human pancreatic cancer. *Oncotarget*, 7(4), 4226-4240.

[55] Dong H., Qian D., Wang Y., Meng L., Chen D., Ji X. & Feng W. (2015). Survivin expression and serum levels in pancreatic cancer. *World J Surg Oncol*, 13, 189.

[56] Li Y., Liu H., Huang Y. Y., Pu L. J., Zhang X. D., Jiang C. C. & Jiang Z. W. (2013). Suppression of endoplasmic reticulum stress-induced invasion and migration of breast cancer cells through the downregulation of heparanase. *Int J Mol Med*, 31(5), 1234-1242.

[57] Shi Z., Wang B., Chihanga T., Kennedy M. A. & Weber G. F. (2014). Energy metabolism during anchorage-independence. Induction by osteopontin-c. *PLoS One*, 9(8), e105675.

[58] Su Z., Yang Z., Xu Y., Chen Y. & Yu Q. (2015). Apoptosis, autophagy, necroptosis, and cancer metastasis. *Mol Cancer*, 14, 48.

[59] Kong B., Wu W., Cheng T., Schlitter A. M., Qian C., Bruns P., Jian Z., Jager C., Regel I., Raulefs S., Behler N., Irmler M., Beckers J., Friess H., Erkan M., Siveke J. T., Tannapfel A., Hahn S. A., Theis F. J., Esposito I., Kleeff J. & Michalski C. W. (2016). A subset of metastatic pancreatic ductal

adenocarcinomas depends quantitatively on oncogenic Kras/Mek/Erk-induced hyperactive mTOR signalling. *Gut*, 65(4), 647-657.

[60] Yamamoto N., Ueda M., Sato T., Kawasaki K., Sawada K., Kawabata K. & Ashida H. (2015). Measurement of glucose uptake in cultured cells. *Curr Protoc Pharmacol*, 71, 1-26.

[61] Schroeder T., Yuan H., Viglianti B. L., Peltz C., Asopa S., Vujaskovic Z. & Dewhirst M. W. (2005). Spatial heterogeneity and oxygen dependence of glucose consumption in R3230Ac and fibrosarcomas of the Fischer 344 rat. *Cancer Res*, 65(12), 5163-5171.

[62] di Magliano M. P. & Logsdon C. D. (2013). Roles for KRAS in pancreatic tumor development and progression. *Gastroenterology*, 144(6), 1220-9.

[63] Liu J., Ben Q. W., Yao W. Y., Zhang J. J., Chen D. F., He X. Y., Li L. & Yuan Y. Z. (2012). BMP2 induces PANC-1 cell invasion by MMP-2 overexpression through ROS and ERK. *Front Biosci (Landmark Ed)*, 17, 2541-2549.

[64] Kim H. S., Kim M. J., Kim E. J., Yang Y., Lee M. S. & Lim J. S. (2012). Berberine-induced AMPK activation inhibits the metastatic potential of melanoma cells via reduction of ERK activity and COX-2 protein expression. *Biochem Pharmacol*, 83(3), 385-394.

[65] Jiao L., Li D. D., Yang C. L., Peng R. Q., Guo Y. Q., Zhang X. S. & Zhu X. F. (2016). Reactive oxygen species mediate oxaliplatin-induced epithelial-mesenchymal transition and invasive potential in colon cancer. *Tumour Biol*, 37(6), 8413-8423.

[66] Kang X., Kong F., Wu X., Ren Y., Wu S., Wu K., Jiang Z. & Zhang W. (2015). High glucose promotes tumor invasion and increases metastasis-associated protein expression in human lung epithelial cells by upregulating heme oxygenase-1 via reactive oxygen species or the TGF-beta1/PI3K/Akt signaling pathway. *Cell Physiol Biochem*, 35(3), 1008-1022.

[67] Mates J. M., Perez-Gomez C. & Nunez de Castro I. (1999). Antioxidant enzymes and human diseases. *Clin Biochem*, 32(8), 595-603.

[68] O'Leary B. R., Fath M. A., Bellizzi A. M., Hrabe J. E., Button A. M., Allen B. G., Case A. J., Altekruse S., Wagner B. A., Buettner G. R., Lynch C. F.,

Hernandez B. Y., Cozen W., Beardsley R. A., Keene J., Henry M. D., Domann F. E., Spitz D. R. & Mezhir J. J. (2015). Loss of SOD3 (EcSOD) Expression Promotes an Aggressive Phenotype in Human Pancreatic Ductal Adenocarcinoma. *Clin Cancer Res*, 21(7), 1741-1751.

[69] Subramani R., Gonzalez E., Arumugam A., Nandy S., Gonzalez V., Medel J., Camacho F., Ortega A., Bonkoungou S., Narayan M., Dwivedi A. & Lakshmanaswamy R. (2016). Nimbolide inhibits pancreatic cancer growth and metastasis through ROS-mediated apoptosis and inhibition of epithelial-to-mesenchymal transition. *Sci Rep*, 6, 19819.

[70] Kong B., Michalski C. W., Hong X., Valkovskaya N., Rieder S., Abiatari I., Streit S., Erkan M., Esposito I., Friess H. & Kleeff J. (2010). AZGP1 is a tumor suppressor in pancreatic cancer inducing mesenchymal-to-epithelial transdifferentiation by inhibiting TGF-beta-mediated ERK signaling. *Oncogene*, 29(37), 5146-5158.

[71] Sureban S. M., May R., Lightfoot S. A., Hoskins A. B., Lerner M., Brackett D. J., Postier R. G., Ramanujam R., Mohammed A., Rao C. V., Wyche J. H., Anant S. & Houchen C. W. (2011). DCAMKL-1 regulates epithelial-mesenchymal transition in human pancreatic cells through a miR-200a-dependent mechanism. *Cancer Res*, 71(6), 2328-2338.

[72] Hotz B., Arndt M., Dullat S., Bhargava S., Buhr H. J. & Hotz H. G. (2007). Epithelial to mesenchymal transition: expression of the regulators snail, slug, and twist in pancreatic cancer. *Clin Cancer Res*, 13(16), 4769-4776.

[73] Rhim A. D., Mirek E. T., Aiello N. M., Maitra A., Bailey J. M., McAllister F., Reichert M., Beatty G. L., Rustgi A. K., Vonderheide R. H., Leach S. D. & Stanger B. Z. (2012). EMT and dissemination precede pancreatic tumor formation. *Cell*, 148(1-2), 349-361.

[74] Camaj P., Jackel C., Krebs S., De Toni E. N., Blum H., Jauch K. W., Nelson P. J. & Bruns C. J. (2014). Hypoxia-independent gene expression mediated by SOX9 promotes aggressive pancreatic tumor biology. *Mol Cancer Res*, 12(3), 421-432.

[75] Ngan C. Y., Yamamoto H., Seshimo I., Tsujino T., Man-i M., Ikeda J. I., Konishi K., Takemasa I., Ikeda M., Sekimoto M., Matsuura N. & Monden M.

(2007). Quantitative evaluation of vimentin expression in tumour stroma of colorectal cancer. *Br J Cancer*, 96(6), 986-992.

[76] Kowalski P. J., Rubin M. A. & Kleer C. G. (2003). E-cadherin expression in primary carcinomas of the breast and its distant metastases. *Breast Cancer Res*, 5(6), R217-222.

[77] Peinado H., Olmeda D. & Cano A. (2007). Snail, Zeb and bHLH factors in tumour progression: an alliance against the epithelial phenotype? *Nat Rev Cancer*, 7(6), 415-428.

[78] Yang X., Takano Y. & Zheng H. C. (2012). The pathobiological features of gastrointestinal cancers (Review). *Oncol Lett*, 3(5), 961-969.

[79] Linder S. & Shoshan M. C. (2005). Lysosomes and endoplasmic reticulum: targets for improved, selective anticancer therapy. *Drug Resist Updat*, 8(4), 199-204.

[80] Firczuk M., Gabrysiak M., Barankiewicz J., Domagala A., Nowis D., Kujawa M., Jankowska-Steifer E., Wachowska M., Glodkowska-Mrowka E., Korsak B., Winiarska M. & Golab J. (2013). GRP78-targeting subtilase cytotoxin sensitizes cancer cells to photodynamic therapy. *Cell Death Dis*, 4, e741.

[81] Whittle M. C., Izeradjene K., Rani P. G., Feng L., Carlson M. A., DelGiorno K. E., Wood L. D., Goggins M., Hruban R. H., Chang A. E., Calses P., Thorsen S. M. & Hingorani S. R. (2015). RUNX3 Controls a Metastatic Switch in Pancreatic Ductal Adenocarcinoma. *Cell*, 161(6), 1345-1360.

[82] Neuzillet C., Tijeras-Raballand A., Cros J., Faivre S., Hammel P. & Raymond E. (2013). Stromal expression of SPARC in pancreatic adenocarcinoma. *Cancer Metastasis Rev*, 32(3-4), 585-602.

[83] Erkan M., Hausmann S., Michalski C. W., Fingerle A. A., Dobritz M., Kleeff J. & Friess H. (2012). The role of stroma in pancreatic cancer: diagnostic and therapeutic implications. *Nat Rev Gastroenterol Hepatol*, 9(8), 454-467.

[84] Whipple C. & Korc M. (2008). Targeting angiogenesis in pancreatic cancer: rationale and pitfalls. *Langenbecks Arch Surg*, 393(6), 901-910.

[85] Qiu B. & Simon M. C. (2015). Oncogenes strike a balance between cellular growth and homeostasis. *Semin Cell Dev Biol*, 43, 3-10.

[86] Yun J., Rago C., Cheong I., Pagliarini R., Angenendt P., Rajagopalan H., Schmidt K., Willson J. K., Markowitz S., Zhou S., Diaz L. A., Jr., Velculescu V. E., Lengauer C., Kinzler K. W., Vogelstein B. & Papadopoulos N. (2009). Glucose deprivation contributes to the development of KRAS pathway mutations in tumor cells. *Science*, 325(5947), 1555-1559.

[87] Colvin E. K. & Scarlett C. J. (2014). A historical perspective of pancreatic cancer mouse models. *Semin Cell Dev Biol*, 27, 96-105.

[88] Son S., Stevens M. M., Chao H. X., Thoreen C., Hosios A. M., Schweitzer L. D., Weng Y., Wood K., Sabatini D., Vander Heiden M. G. & Manalis S. (2015). Cooperative nutrient accumulation sustains growth of mammalian cells. *Sci Rep*, 5, 17401.

[89] Konstantakou E. G., Voutsinas G. E., Velentzas A. D., Basogianni A. S., Paronis E., Balafas E., Kostomitsopoulos N., Syrigos K. N., Anastasiadou E. & Stravopodis D. J. (2015). 3-BrPA eliminates human bladder cancer cells with highly oncogenic signatures via engagement of specific death programs and perturbation of multiple signaling and metabolic determinants. *Mol Cancer*, 14, 135.

[90] Kwon S. J. & Lee Y. J. (2005). Effect of low glutamine/glucose on hypoxia-induced elevation of hypoxia-inducible factor-1alpha in human pancreatic cancer MiaPaCa-2 and human prostatic cancer DU-145 cells. *Clin Cancer Res*, 11(13), 4694-4700.

[91] Belkacemi L., Lam E., Caldwell J. D., Siemens D. R. & Graham C. H. (2006). Stimulation of human breast carcinoma cell invasiveness and urokinase plasminogen activator activity by glucose deprivation. *Exp Cell Res*, 312(10), 1685-1692.

[92] Birsoy K., Possemato R., Lorbeer F. K., Bayraktar E. C., Thiru P., Yucel B., Wang T., Chen W. W., Clish C. B. & Sabatini D. M. (2014). Metabolic determinants of cancer cell sensitivity to glucose limitation and biguanides. *Nature*, 508(7494), 108-112.

[93] Dibble C. C. & Manning B. D. (2013). Signal integration by mTORC1 coordinates nutrient input with biosynthetic output. *Nat Cell Biol*, 15(6), 555-564.

[94] Dolado I. & Nebreda A. R. (2008). AKT and oxidative stress team up to kill cancer cells. *Cancer Cell*, 14(6), 427-429.

[95] Sullivan L. B. & Chandel N. S. (2014). Mitochondrial reactive oxygen species and cancer. *Cancer Metab*, 2, 17.

[96] Long J. S. & Ryan K. M. (2012). New frontiers in promoting tumour cell death: targeting apoptosis, necroptosis and autophagy. *Oncogene*, 31(49), 5045-5060.

[97] Satoh K., Hamada S. & Shimosegawa T. (2015). Involvement of epithelial to mesenchymal transition in the development of pancreatic ductal adenocarcinoma. *J Gastroenterol*, 50(2), 140-146.

[98] Li Z., Guo J., Xie K. & Zheng S. (2015). Vitamin D receptor signaling and pancreatic cancer cell EMT. *Curr Pharm Des*, 21(10), 1262-1267.

[99] Van de Casteele M., Kefas B. A., Cai Y., Heimberg H., Scott D. K., Henquin J. C., Pipeleers D. & Jonas J. C. (2003). Prolonged culture in low glucose induces apoptosis of rat pancreatic beta-cells through induction of c-myc. *Biochem Biophys Res Commun*, 312(4), 937-944.

[100] Caro-Maldonado A., Tait S. W., Ramirez-Peinado S., Ricci J. E., Fabregat I., Green D. R. & Munoz-Pinedo C. (2010). Glucose deprivation induces an atypical form of apoptosis mediated by caspase-8 in Bax-, Bak-deficient cells. *Cell Death Differ*, 17(8), 1335-1344.

[101] Kretowski R., Stypulkowska A. & Cechowska-Pasko M. (2013). Low-glucose medium induces ORP150 expression and exerts inhibitory effect on apoptosis and senescence of human breast MCF7 cells. *Acta Biochim Pol*, 60(2), 167-173.

[102] Jung S., Li C., Duan J., Lee S., Kim K., Park Y., Yang Y., Kim K. I., Lim J. S., Cheon C. I., Kang Y. S. & Lee M. S. (2015). TRIP-Br1 oncoprotein inhibits autophagy, apoptosis, and necroptosis under nutrient/serum-deprived condition. *Oncotarget*, 6(30), 29060-29075.

[103] Weis S. M. & Cheresh D. A. (2011). Tumor angiogenesis: molecular pathways and therapeutic targets. *Nat Med*, 17(11), 1359-1370.

[104] Kong B., Cheng T., Wu W., Regel I., Raulefs S., Friess H., Erkan M., Esposito I., Kleeff J. & Michalski C. W. (2015). Hypoxia-induced

endoplasmic reticulum stress characterizes a necrotic phenotype of pancreatic cancer. *Oncotarget*, 6(31), 32154-32160.

[105] Satake S., Kuzuya M., Miura H., Asai T., Ramos M. A., Muraguchi M., Ohmoto Y. & Iguchi A. (1998). Up-regulation of vascular endothelial growth factor in response to glucose deprivation. *Biol Cell*, 90(2), 161-168.

[106] de Laplanche E., Boudria A., Dacheux E., Vincent A., Gadot N., Assade F., Le Corf K., Leroy X., Mege Lechevallier F., Eymin B., Dalla Venezia N. & Simonnet H. (2015). Low glucose microenvironment of normal kidney cells stabilizes a subset of messengers involved in angiogenesis. *Physiol Rep*, 3(1), e12253.

[107] Biadgo B. & Abebe M. (2016). Type 2 Diabetes Mellitus and Its Association with the Risk of Pancreatic Carcinogenesis: A Review. *Korean J Gastroenterol*, 67(4), 168-177.

[108] Eizirik D. L., Korbutt G. S. & Hellerstrom C. (1992). Prolonged exposure of human pancreatic islets to high glucose concentrations in vitro impairs the beta-cell function. *J Clin Invest*, 90(4), 1263-1268.

[109] Dima S. O., Tanase C., Albulescu R., Herlea V., Chivu-Economescu M., Purnichescu-Purtan R., Dumitrascu T., Duda D. G. & Popescu I. (2012). An exploratory study of inflammatory cytokines as prognostic biomarkers in patients with ductal pancreatic adenocarcinoma. *Pancreas*, 41(7), 1001-1007.

[110] Parker W. P., Cheville J. C., Frank I., Zaid H. B., Lohse C. M., Boorjian S. A., Leibovich B. C. & Thompson R. H. (2017). Application of the Stage, Size, Grade, and Necrosis (SSIGN) Score for Clear Cell Renal Cell Carcinoma in Contemporary Patients. *Eur Urol*, 71(4), 665-673.

[111] Costa-Silva B., Aiello N. M., Ocean A. J., Singh S., Zhang H., Thakur B. K., Becker A., Hoshino A., Mark M. T., Molina H., Xiang J., Zhang T., Theilen T. M., Garcia-Santos G., Williams C., Ararso Y., Huang Y., Rodrigues G., Shen T. L., Labori K. J., Lothe I. M., Kure E. H., Hernandez J., Doussot A., Ebbesen S. H., Grandgenett P. M., Hollingsworth M. A., Jain M., Mallya K., Batra S. K., Jarnagin W. R., Schwartz R. E., Matei I., Peinado H., Stanger B. Z., Bromberg J. & Lyden D. (2015). Pancreatic

cancer exosomes initiate pre-metastatic niche formation in the liver. *Nat Cell Biol*, 17(6), 816-826.

[112] Paron I., Berchtold S., Voros J., Shamarla M., Erkan M., Hofler H. & Esposito I. (2011). Tenascin-C enhances pancreatic cancer cell growth and motility and affects cell adhesion through activation of the integrin pathway. *PLoS One*, 6(6), e21684.

9. SUPPLEMENTARY DATA

Supplemental Table 1. The top-100 differentially expressed genes in Mek/Erk-dependent cell line 399

Gene	logFC	adj.P.Val
Glod5	-3.444740418	0.001889209
Efemp1	-3.350300078	0.000220681
2310042E22Rik	-2.78574195	0.000220681
Gucy1a2	-2.676939759	0.00142905
Isx	-2.670675177	0.001660454
Ddc	-2.643221962	0.000220681
Dio3os	-2.171123762	0.002805137
Ceacam1	-2.164123541	0.000657925
S100g	-2.147937037	0.001660454
Rab6b	-2.0604725	0.000568107
Cst9	-2.002434206	0.005525446
Pmp22	-1.991985927	0.006924993
Cldn3	-1.984128121	0.014989437
Ocln	-1.857143348	0.001466054
Mcpt2	-1.797004244	0.00607576
Tmigd1	-1.779019884	0.001560663
Gda	-1.776972675	0.001660454
Rasef	-1.742254909	0.00142905

Slco2a1	-1.740922462	0.002808999
Hoxa13	-1.636680109	0.000750801
Hpse	-1.58806993	0.003899911
BC030870	-1.568049001	0.002805137
Tgfb1i1	-1.522080635	0.001660454
Ildr2	-1.504144436	0.001466054
Mst1r	-1.490960839	0.001466054
Ivl	-1.47196463	0.167374561
Nlrc4	-1.463328791	0.006669106
Tmprss2	-1.4551849	0.015293587
Gm20744	-1.454056148	0.008808688
Tff1	-1.392204978	0.091683109
Arap3	-1.377190788	0.001890871
Serpinb1a	-1.373395913	0.006383585
Gnai1	-1.366435311	0.008024358
Csn3	-1.351046235	0.00500164
Mir680-2	-1.347239265	0.003321833
Cmtm8	-1.343461881	0.002808999
Sh2d4a	-1.338041788	0.00415026
Ptgs1	-1.317936326	0.00172986
Elf3	-1.300299138	0.001729125
Atp7b	-1.292535567	0.024073704

Rnf128	-1.269690066	0.012866844
Tmlhe	-1.239079357	0.036199242
Ccdc3	-1.230684676	0.036199242
Erbb3	-1.215199508	0.018749175
Mal	-1.202576514	0.011791712
Rps6ka2	-1.187685677	0.035817771
Hs3st5	-1.18520946	0.003321833
Acan	-1.184840536	0.008005769
Fbp2	-1.169236648	0.105481547
Cst13	-1.16363786	0.03611691
Sgpp2	-1.15744886	0.10127505
Anxa10	-1.144343369	0.135654843
Tnfsf15	-1.127774695	0.003672817
Calcb	-1.099426158	0.032978432
Cyp2c65	-1.096151028	0.048014521
9930013L23Rik	-1.091885909	0.040259981
Tmtc2	-1.087003243	0.041155169
Arl14	-1.076910019	0.026150753
Rcn1	-1.075871773	0.183741951
Renbp	-1.075386716	0.023519826
Tns1	-1.072032113	0.052105449
Cdc42ep3	-1.057443325	0.018931827

Epn3	-1.055345369	0.105481547
Hoxa10	-1.050179958	0.005008781
Lamc2	-1.048895426	0.040196406
Hoxa5	-1.047917425	0.027805913
Epb4.1l4a	-1.044666962	0.02168726
Myo1b	-1.043949611	0.00867382
Cyba	-1.042387059	0.094799182
Nrep	-1.042353382	0.159184838
Rhox5	-1.04191013	0.030838058
Snap25	-1.036166323	0.079087103
Krt13	-1.033560508	0.104142607
Aqp1	-1.031001197	0.049755021
Dtna	-1.024386633	0.023367518
Tspan13	-1.017904237	0.007764371
Gm4340	-1.017406896	0.190369364
Xlr3a	-1.005556335	0.040854263
Col6a1	1.000240249	0.023367518
Sesn3	1.003254285	0.015099967
H2afy2	1.011135563	0.160009936
Sgcb	1.017844002	0.008817485
Gm13251	1.030586751	0.020581213
Sult1c2	1.054708287	0.211217351

Timp3	1.059986356	0.125709447
Pcdhb17	1.067274581	0.018669099
Lphn1	1.075938508	0.015099967
Usp27x	1.08776339	0.007912982
H1fx	1.095259422	0.047194534
Dyrk1b	1.095473723	0.235685854
Blnk	1.100605157	0.015099967
Mr1	1.105168414	0.158561202
Ak5	1.128038568	0.071169558
Cxxc5	1.132675	0.047194534
Fjx1	1.139393517	0.048853803
Nradd	1.153925869	0.015099967
Baalc	1.159833054	0.096782763
Plxnd1	1.174481143	0.015099967
Ttc12	1.187839357	0.014232982
Apobr	1.21576697	0.04989587

Supplemental Table 2. The top-100 differentially expressed genes in PI3K/Akt-dependent cell line 926

Gene	logFC	adj.P.Val
Ctla2b	-5.44898167	2.08E-05
Ctla2a	-5.374927267	2.56E-05
Il11	-5.307466523	8.57E-06
4930486L24Rik	-5.044585442	1.23E-06
Elmod1	-4.713399644	1.47E-05
Ly6a	-4.639704746	0.000913147
Inhba	-4.582136263	0.000116596
Gpr115	-4.272388631	0.00012647
Dpysl3	-4.259703571	6.65E-05
Apol9b	-4.240086855	0.000894838
Timp3	-4.109301131	0.000131115
Mmp10	-4.107381145	0.000218276
Rcn1	-4.0980128	1.42E-05
Tspan6	-3.936229941	3.74E-06
Ddx3y	-3.882044323	0.000119125
Thbs1	-3.676968618	0.000204388
Exo5	-3.652704464	9.03E-06
Gpx8	-3.614164674	1.01E-05
Layn	-3.544211499	1.01E-05

Gli3	-3.513012225	7.49E-06
Eda2r	-3.379270077	9.20E-05
Gm6634	-3.37150201	0.001017266
Col12a1	-3.326002939	4.95E-05
Snai2	-3.322084156	0.000558645
Lrch2	-3.229000174	2.01E-05
Gc	-3.227843092	0.000539804
Khdrbs3	-3.18227351	8.08E-05
Crip2	-3.177200135	7.39E-06
Lmcd1	-3.131195813	0.000116596
Casc4	-3.123188517	0.000138467
Nes	-3.094566986	4.97E-05
Tmlhe	-3.0679806	2.11E-05
Prdx4	-3.000660291	2.87E-05
Scn5a	-2.984980765	3.28E-05
Sulf2	-2.964353214	9.25E-05
Piezo2	-2.950626336	0.00028539
Mcpt8	-2.926698475	1.01E-05
Stk39	-2.910104859	0.008108194
Plscr2	-2.881888418	1.01E-05
Igfbp3	-2.874774134	1.74E-05
Pde3b	-2.8580202	1.27E-05

Adam23	-2.857342543	0.000142223
F2r	-2.854238944	3.38E-05
Eif2s3y	-2.82840987	7.08E-05
Nbea	-2.684926068	0.000154774
Jph1	-2.672855798	7.08E-05
9930111J21Rik2	-2.667726915	0.010845655
Areg	-2.657996481	0.008231784
Edn1	-2.597074484	0.012749772
Lect2	-2.584418567	0.006656238
Ankrd1	-2.578551679	0.000124205
Atf3	-2.569682453	0.045938058
Cxcl12	-2.566614021	4.51E-05
Tmeff1	-2.55272172	0.010725543
Leprel1	-2.544610764	3.38E-05
Gpr141	-2.496051028	0.04909082
Cdca7l	-2.468644803	3.68E-05
Masp1	-2.462891878	1.01E-05
Atp11a	-2.436161426	0.000142852
Lamb1	-2.416518592	0.000119811
Gdf15	-2.416157855	0.0036955
Trib3	-2.360753679	0.022349578
Glipr2	-2.354206659	0.000842395

Ddit3	-2.332626126	0.022771059
Sgcb	-2.316600479	0.00016128
Kcnn3	-2.311291655	0.002234191
Tnnt2	-2.3075417	0.000170558
Cd109	-2.295623105	0.000233375
Crlf1	-2.290873468	9.20E-05
Serpina1c	-2.27717455	0.063792744
Cth	-2.276785311	0.064848471
Serpine1	-2.273334036	0.001591546
Cd53	-2.249607136	0.023240876
Serpinh1	-2.24855108	6.24E-05
Eif4e3	-2.238731818	0.000317521
Pdlim1	-2.225578321	4.67E-05
Six1	-2.22304892	6.49E-05
Ctgf	-2.219782022	0.000700173
Nnmt	-2.210401274	0.010157668
Kdelr3	-2.18147569	0.000397195
AK129341	-2.166589457	0.00452317
Otud1	-2.165745224	0.000738324
Kdm5d	-2.146715955	0.000218276
Plod2	-2.135905968	9.46E-05
Cnn2	-2.126577166	3.72E-05

Wisp1	-2.124172632	0.000271039
Ifi27l2b	-2.122858408	0.001465698
Frmd6	-2.097781059	4.51E-05
Tbx18	-2.084389838	0.001152217
Olfr877	-2.07067447	0.010515656
4930461G14Rik	-2.068096062	0.134817979
Gm11714	-2.055168586	0.101837194
Cda	-2.053555877	0.00104981
Zak	-2.042296783	5.05E-05
Jag1	-2.032728182	0.00136963
Plk2	-2.027665227	0.000338516
Anxa6	-2.027508921	0.000558562
Wars	-2.019815853	0.006133673
Lif	-2.00018944	0.001104993
Tubb3	-1.99116071	0.005408839

10. CURRICULUM VITAE

Familienname: Jian

Vorname: Ziying

Geburtsdatum: 29.07.1986

Geschlecht: weblich

Familienstatus: Single

Nationalität: Chinese

Adresse: Plettstr. 39, c/o Shi , 81735 München

Tel: 015166035539

Email: jianziying86729@hotmail.com

Ausbildung und beruflicher Werdegang:

12/2012-Stipendiat, Anfertigung der medizinischen Doktorarbeit, Technische Universität München

09/2010 -06/2012   Master in Medizin, Southeast University, China

09/2005 -06/2010   Bachelor in Medizin, Southeast University, China

Publikationen:

Kong B, Wu W, Cheng T, Schlitter AM, Qian C, Bruns P, Jian Z, et al. A subset of metastatic pancreatic ductal adenocarcinomas depends quantitatively on oncogenic Kras/Mek/Erk-induced hyperactive mTOR signalling. Gut. 2016 Apr;65(4):647-657

11. ACKNOWLEDGEMENTS